RSC Advances

REVIEW

View Article Online
View Journal | View Issue

Cite this: *RSC Adv.*, 2026, **16**, 19802

Recent development of active metallic nanostructures-encapsulated carbon hybrid materials for ORR, OER, and HER applications

Nguyen Chi Thanh *

The search for cost-effective, abundant, and efficient alternatives to precious metal catalysts is vital for advancing electrocatalytic performance. Despite various studies on non-precious metal catalysts, their industrial application remains hindered by their inherent reactivity and poor stability. A promising strategy, based on encapsulating non-precious active metal materials within 2D carbon supporting materials, offers distinct benefits, including improved catalytic performance and long-term durability. Such behaviors are attributed to their synergistic effect, which provides ample electrochemically active sites, tunable electronic properties, and an innovative structural design that enhances interaction between the constituents. This review summarizes the recent progress in preparation methods, innovative micro/nano structures, and the widespread applications of nonprecious metal-derived electrocatalysts confined within two-dimensional carbon layers. The main merits and demerits of various synthesis strategies will be critically evaluated to elucidate the relationship between structure and properties, with the aim of improving electrochemical performance. Furthermore, this review highlights the significance of these hybrids for various potential electrochemical processes, including the oxygen evolution reaction (OER), hydrogen evolution reaction (HER), and oxygen reduction reaction (ORR), in the context of relevant fuel cells, metal–air batteries, and water electrolysis. Lastly, the existing issues in the primary study, their practicality, and prospective directions for future development are also briefly emphasized.

Received 17th January 2026
Accepted 31st March 2026

DOI: 10.1039/d6ra00427j

rsc.li/rsc-advances

Introduction

Nanocatalysis, due to its superior activity and durability, serves as a crucial tool in modern science and technology. In this context, the most well-known precious metal catalysts, made from Pt, Pd, or Ru, are advanced catalysts that have been extensively applied in various areas of electrochemical applications due to their superior catalytic behaviour, selectivity, and stability, surpassing traditional nanomaterials. However, the most significant challenge to their large-scale industrial implementation is their limited availability, which drives up costs.[1,2] Furthermore, although stable, precious metal catalysts can still degrade over time due to structural changes triggered by undesirable oxidation, carbon support corrosion, and migration, resulting in a loss of surface area.[3] There is a pressing need to address the high-cost challenge posed by precious-metal catalysts to the practical realization of related technologies, such as fuel cells and green hydrogen production. In this aspect, various strategies have been implemented, including the efficient utilization of Pt, improved recycling methods, and the complete replacement of Pt.[4,5] Alternatively, significant efforts are being made to develop catalysts with superior physicochemical properties using either Pt alternatives or coupling with other precious metals (alloys).[6–8] Although this approach, which utilizes inexpensive Pd, Ru, or their alloys, is viable, it is not suitable for long-term adoption in practical applications due to its limited activity and poor availability. Another promising, inexpensive route with high abundance and uniform worldwide distribution is the utilization of transition metals (TMs) with various established structures, including hydroxides, carbides, oxides, sulfides, selenides, borides, and nitrides.[9–12] Although extensive progress has been made in their development, several challenges persist due to their inherent reactivity, resulting in poor stability, low electrical conductivity, and reduced activity.[13] Consequently, two-dimensional (2D) conducting supports anchored with TMs have gained attention as promising candidates for the development of catalysts,[14–16] which can be fabricated using top-down and bottom-up approaches, including hydrothermal synthesis, chemical reactions, and electroplating.[17–23] These, together with the rise of carbon allotropes having unique structural properties, *i.e.*, large surface area, high mechanical strength, and facile functionalization, such as two-dimensional (2D) graphitic carbon nitride ($g\text{-}C_3N_4$) and graphene sheets (GNS), can create advanced

Faculty of Applied Sciences, Ho Chi Minh City University of Technology and Engineering, 01 Vo Van Ngan Street, Thu Duc Ward, Ho Chi Minh City, Vietnam. E-mail: thanhnc@hcmute.edu.vn

hybrid materials with desirable characteristics in electrocatalysis applications.[24–26] Nevertheless, simply loading active metal catalysts onto 2D carbon surfaces often fails to establish strong interfacial interactions between the two components, leading to accumulation and leaching that ultimately result in insufficient catalytic activity and poor durability.[27] The design of a nanoarchitecture that ensures specific, strong interactions between TMs and 2D-carbon-based supports by modulating their (metals and carbon) electronic environments is highly regarded as a promising method for achieving inexpensive, efficient catalysts that surpass the performance of precious-metal catalysts in electrochemical applications.[28,29] Interestingly, core–shell nanostructures featuring active nanomaterials encapsulated within 2D carbon allotropes with tailored functionalities have emerged as advanced candidates for diverse electrochemical applications.[30–35] The enhanced catalytic activity and stability of these systems arise from the unique interactions between active metal carbon shells to form efficient conductive networks, improve interfacial contact, and suppress nanoparticle self-agglomeration.[36–39] Moreover, the geometric configuration of these nanostructures helps mitigate the volume increase and prevents leaching of the inorganic components during the working process. Thus, the core–shell architecture enhances the electrochemical surface area and increases the number of active centers, resulting in superior catalytic activity.

Recently, many review articles have extensively covered hybrid systems of carbon allotropes and TM catalysts.[40–43] Although these comprehensive reviews have focused well on the promising contributions of core–shell TM@C electrocatalysts in electrocatalytic applications, the insight into the influence of morphology and the correlation between structure and physicochemical properties on the electrochemical behaviour of various transition metal types encapsulated by a carbon layer has not yet been emphasized. To bridge this gap, this review provides a detailed insight into the research progress in TM@C hybrids, focusing on their systematic synthesis approach, structure–electrochemical properties relationships, and prospective electrochemical applications. Furthermore, we highlight the current challenges, scope for academic research, and summarize their potential for practical implementation. We believe this review provides a focused perspective on the development of advanced catalysts and will also serve as a knowledge base for global researchers dedicated to the development of novel nanomaterials for electrochemical applications.

2D carbon allotrope materials

Since the groundbreaking 2004 discovery and isolation of GNS using the "Scotch Tape process" of mechanical exfoliation by Geim and Novoselov, intense investigation on 2D nanostructured materials has advanced rapidly across diverse research areas, such as materials science and nanotechnology, due to their unique physicochemical behavior, contradicting their bulk counterparts.[24,44,45] Within this context, we present a brief discussion of emerging 2D carbon allotropes, including g-C_3N_4 and GNS, which hold great promise for various fields due to their unique properties that enable them to serve as both active and supporting components for innovative electrochemical applications. g-C_3N_4 is a polymeric semiconductor that is held together *via* van der Waals forces. This structure is created by stacking sheets of C and N. Here, the lattice consists of a hexagonal carbon configuration substituted by N *via* the sp^2 hybridization of C and N atoms. Among the various forms of carbon nitride, g-C_3N_4 is regarded as the most thermodynamically stable allotrope.[46] Its synthesis typically involves thermal polymerization of N-rich precursors, such as urea, cyanamide, melamine, thiourea (CH_4N_2S), and dicyandiamide (Fig. 1a).[44,47,48] Variations in N source choice and reduction pathways yield g-C_3N_4 with specific structures. Specifically, g-C_3N_4 could be constructed from the condensation of *s*-triazine (C_3N_3) units or *s*-heptazine (C_6N_7).[49–51] The N incorporation endows g-C_3N_4 with special surface characteristics, including highly structural defects, diverse surface functional groups, and charge–rich properties. These improve its interactions with intermediates during electrocatalytic reactions. Furthermore, g-C_3N_4 exhibits excellent physicochemical stability, which is extremely favorable for catalytic and heterogeneous catalytic applications (Fig. 1b).[47] Due to its semiconducting nature and a unique band gap of approximately 2.7 eV, g-C_3N_4 is a promising material for photocatalysis. In particular, heptazine-based g-C_3N_4 serves as both an active component and a robust substrate for diverse electrochemical processes.[44,48] When hybridized with active metals, g-C_3N_4 can alter the electronic states and ΔG_{H^*} at the interfacial regions, thereby promoting electron transfer and significantly enhancing electrochemical activity.[52]

Graphene, a 2D sheet of sp^2-hybridized C atoms forming a honeycomb lattice, which acts as the primary building block for various graphitic carbon nanostructures (Fig. 1c).[53] The remarkable attention in GNS is attributed to its exceptional features, including a very high theoretical surface area (2630 m^2 g^{-1}), outstanding thermal conductivity (~5000 W m^1 K^1), superior Young's modulus (~1100 GPa), and fracture strength (125 GPa). Moreover, GNS exhibits a zero-bandgap architecture, displaying excellent electrical conductivity (Fig. 1d).[24,45,53] Interestingly, its electronic and structural features could be further modulated by creating a stacking heterostructure with zero-dimensional, one-dimensional, or other two-dimensional materials.[54–58] Such hybrid materials could be horizontally constructed *via* covalent interactions, ensuring excellent in-plane strength, or vertically stacked *via* weak van der Waals interactions, thus creating a specific heterojunction. Additionally, defect engineering and heteroatom doping represent efficient strategies for modulating the physicochemical and electronic behavior of GNS.[59,60] It is well established that edge defects and electronic states localized at defect sites are highly active for electrocatalysis.[61] Beyond defects, heteroatom doping—by substituting sp^2 carbon atoms with S, N, P, F, or B—has proven effective in tailoring the properties of GNS to improve its functions.[62,63] Therefore, GNS demonstrates a great potential across diverse applications, including electronics, energy and conversion, bioengineering, and polymer

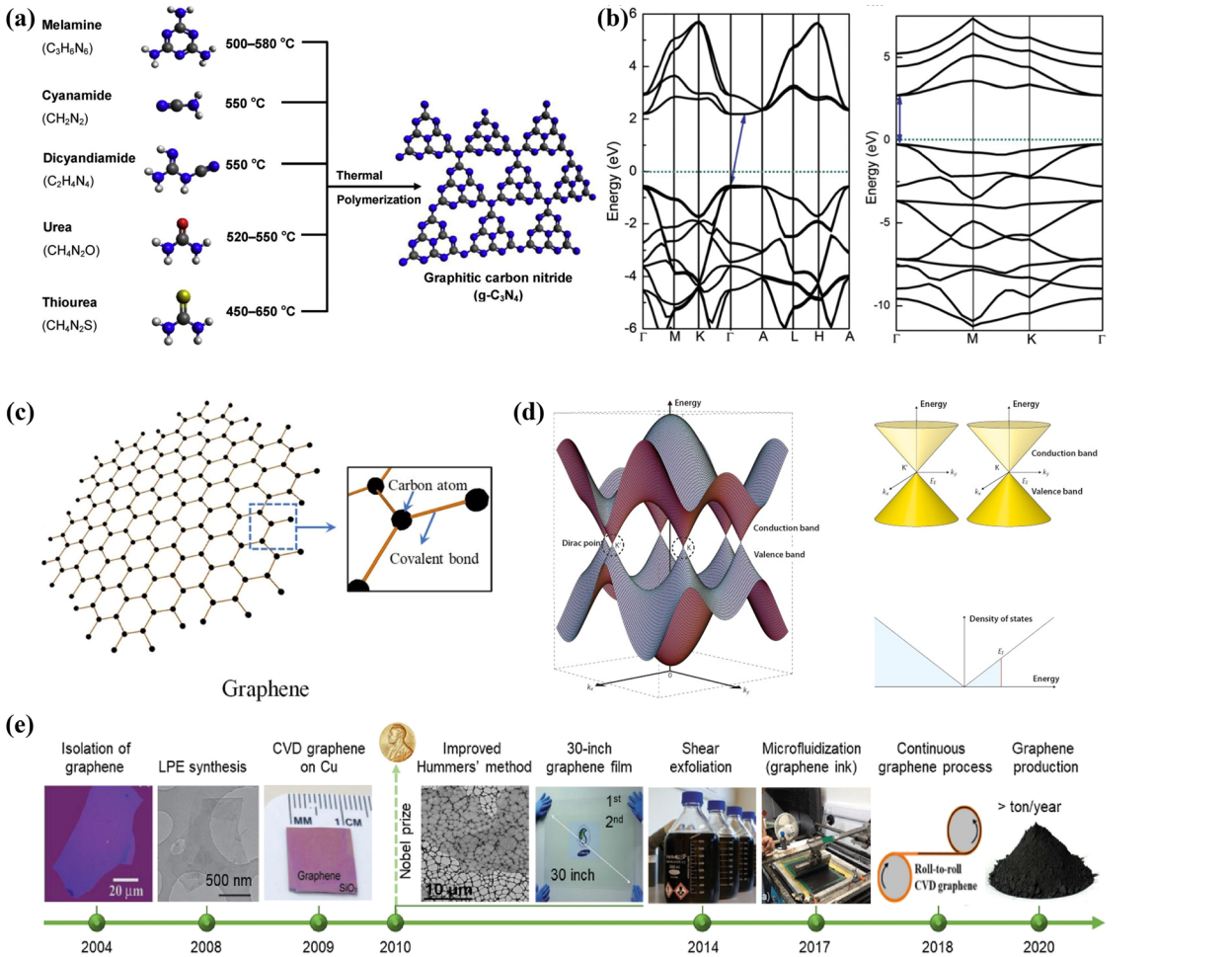

Fig. 1 (a and b) Synthesis, structure, and electronic properties of g-C_3N_4 material (reproduced from ref. 47 with permission from Elsevier, copyright 2022); (c) structure and (d) electronic properties of GNS material[53] (Copyright from MDPI); (e) synthesis timeline of GNS material (reproduced from ref. 69 with permission from Springer, copyright 2009).

nanocomposites.[64–68] Accordingly, diverse preparation routes, such as chemical vapor deposition (CVD), plasma-assisted CVD, chemical exfoliation, or arc discharge, have been reported to produce a variety of GNS types with tailored properties for specific applications (Fig. 1e).[69] While bottom-up-synthesized GNS with high-quality structure and excellent conductivity has attracted considerable attention for high-performance electronic devices, chemically synthesized GNS is promising for polymer nanocomposites and electrocatalysis due to its scalability, high surface area, and functionality.[70]

Active TM catalysts and advances of their core–shell hybrids with 2D carbon

Transition metals, including Fe, Co, Mn, V, Cr, and Ni… are widely used as "non-precious catalysts" owing to their cost-effectiveness, earth-abundance, and environmental friendliness. Specifically, as shown in Fig. 2a, TMs found in groups 4 through 8 of the periodic table, including Cr, V, and Mn, have gained significant attention from global research groups for catalysis due to their interesting physicochemical behavior.[71] In 1964, Raymond Jasinski introduced the role of Co-phthalocyanine towards the oxygen reduction reaction (ORR) in alkaline.[72] His groundbreaking discovery laid the foundation for advanced research into non-precious metals for electrocatalysis. Later in 1970, a notable investigation by Morcos and Yeager on the role of metal-N4 macrocycles in supporting superior area carbon materials laid the foundational step in deciphering such materials. Despite the multitude of discoveries being made, the inherent reactivity of TMs was insufficient to replace Pt.[73] With gratitude for the year 2005, the advancements related to stringent control over the catalyst layer structure and porosity have enabled the TMs catalysts to overcome the limitations of both activity and stability.[74,75] Every advancement introduces new obstacles, such as active site dissolution and leaching, as well as oxidation influence, requiring new strategies to overcome them. In this context, compositional engineering of TMs utilizing innovative fabrication approaches is being explored, including oxides, hydroxides, phosphides, carbides, sulfides, and nitrides. These materials have merits, including superior conductivity and

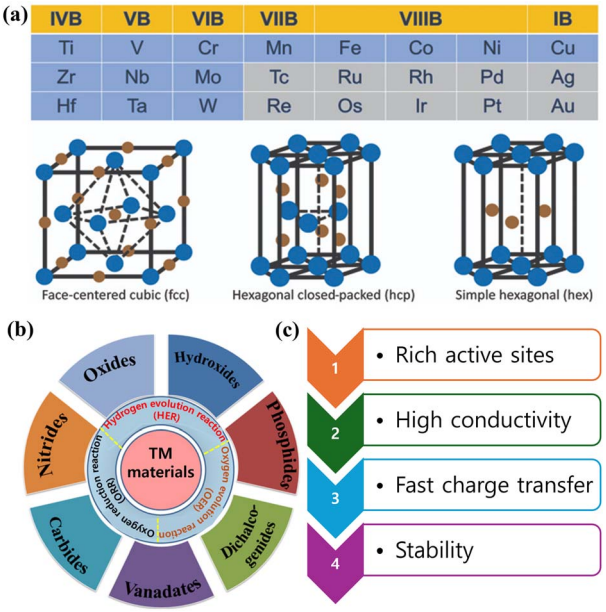

Fig. 2 (a) Different potential transition metals in Group IVB to IB highlighted in blue for catalyst development (reproduced from ref. 71 with permission from AAAS, copyright 2022); (b) various potential TM-based materials, such as oxides, hydroxide, phosphides, di-chalcogenides, carbides, and nitrides, and (c) their unique properties for electrochemical applications (reproduced from ref. 76 with permission from MDPI, copyright 2024).

catalytic activity, making them suitable for electrochemical applications (Fig. 2b, c and Table 1).[76] The deliberate insertion of O, C, P, or N heteroatoms in TMs causes tuning in their electronic properties, metal lattice structure, and interatomic spacing, enhancing the density of states (DOS) and d-band broadening, while adopting fcc, hcp, or simple hexagonal structures.[77–79] The fabrication of nanostructured TM-based catalysts results in notable changes in their physical, chemical, and mechanical properties.[80,81] Particularly, morphology modulation affects lattice microstrain, defect generation, and edge density, thereby increasing surface vacancies and tuning the interaction between the catalyst and reactants.[82,83] A previous investigation has revealed that the particle structure of the active catalysts has a proportional influence on adsorption behavior towards the reactants.[84] Zhao and coauthors developed a NiO flower-like nanostructure with a large surface area and uniform pore size distribution, thereby achieving superior activity compared to NiO nanoparticles. Such performance was attributed to the structure–property relationships with a flower-like morphology, which provided coordinatively unsaturated Ni atoms, rich defect sites, and a higher density of oxygen vacancies, thereby creating an ample number of active sites and stronger interactions with the reactants.[85]

It is essential to note that 3d-transition metals, particularly Ni, Co, and Fe, have been the focus of research and development over the past decade, serving as alternatives to Pt-group metal nanomaterials. Despite their advantages, they suffer from several challenges, including inactivation caused by metal dissolution and accumulation in harsh operating conditions. Therefore, it's necessary to explore new avenues for research. Extensive research indicates that a carbon structure with N-functionalization can enhance its immobilization and strength towards metal catalysts; however, such methods offer only limited effectiveness. In comparison, engineering well-defined nanostructures based on active metal species-coated 2D carbon sheets has emerged as a far more effective strategy, delivering greatly enhanced stability without compromising catalytic activity. In recent years, such encapsulation strategies have been employed to fabricate TM compounds, yielding intriguing achievements in terms of morphology and physico-chemical properties. In this review, we highlight pioneering research on core–shell hybrids, focusing on innovations that enhance the structure and catalytic behaviour for various applications.

TMs confined by 2D carbon materials

A potential design for catalysts based on TMs-coated carbon matrices creates unique physicochemical properties that offer advantages, particularly in improving electrochemical performance. A recent study demonstrated that Co NPs can be uniformly encapsulated within N-doped GNS shells (Co@NGNS).[86] The Co NPs exhibited an average diameter of 8.40 ± 0.19 nm and were completely enclosed by GNS with a thickness of approximately 5 nm or less. The presence of Co metal and highly crystalline carbon, with no visible other Co-based compounds, as confirmed by X-ray diffraction (XRD), leads to exciting behaviors in oxidative dehydrogenation and hydrogenation reactions. In addition, a similar core–shell nanoarchitecture using Co NPs wrapped within GNS shells was also reported by Liu and coauthors.[87] Fu and coauthors designed an interesting nanostructure with Ni NPs integrated within a 3–4-layer g-C_3N_4 framework. This morphology enhances performance by creating abundant active centers for hydrogen adsorption and the subsequent activation of the CN group for catalysis, without being physically involved in the reaction environment, thereby blocking mass loss, poisoning, and acid corrosion of Ni NPs.[88,89] These studies were further implemented on Ni@GNS to achieve long-term durability in a harsh electrolyte.[90] The construction of microsphere architectures in which an ultrathin GNS shell encapsulates regular metallic Ni NPs indicates the formation of Ni NPs, all below 15 nm in size, fully confined within 2–6 nm thick GNS shells, forming well-defined microspheres.[91] Similarly, 2D carbon-encapsulated TM NPs, including Ni-encapsulated C and Co-encapsulated N–C,[92,93] have exhibited remarkable electrocatalytic activity coupled with exceptional durability. Nevertheless, the optimum exposure of TMs' active sites for catalysis can be achieved by stringently regulating the carbon shell's thickness. To support the above notion, Zhang and coauthors designed Cu NPs encapsulated by GNS shell of 1–2 nm thickness (Fig. 3a–c).[94] Copper (Cu) has shown the potential in terms of cost and conductivity to surpass precious metals in conductive inks. However, its tendency to oxidize at ambient room temperature limits its practical application. The study from Wang and coauthors specifically offered a solution *via* the

Table 1 Common types of transition-metal compounds and their key advantages and limitations for electrocatalysis

Transition metal compounds	Abbreviated name	Key advantages and limitations
Transition metal oxides	TMOs	- Abundant and cheap raw materials suitable for low-cost electrocatalysis, good OER activity due to variable oxidation states, and prospective corrosion resistance during OER - Low conductivity; poor reaction kinetics; limited structural stability with dissolution, sintering…
Transition metal hydroxides	TMHOs	- Abundance and low-cost catalysts, large surface area due to formation of unique morphology and structural flexibility, and outstanding stability in alkaline medium - Low conductivity, insufficient durability during long-term operation due to structural collapse or dissolution/sintering, poor catalytic behavior in acid medium, and low thermal stability
Transition metal nitrides	TMNs	- High conductivity with noble metal-like electronic structure, good chemical and thermal stability, and corrosion resistance in acidic or alkaline environments, tunable structure/composition - Undergo surface oxidation under highly oxidizing potentials during OER, a complicated synthesis strategy, agglomeration during synthesis, and reducing the effective surface
Transition metal carbides	TMCs	- Remarkable chemical stability in harsh electrolytes, high conductivity with tunable activity, and noble metal-like behavior, similar to Pt for HER - Challenges of the synthesis strategy with the requirement of high temperature, surface oxidation leading to reduced stability during operation
Transition metal sulfides	TMSs	- Abundance with cost effectiveness, excellent HER/OER activity in alkaline media, outstanding charge mobility and charge transfer kinetics, structural tunability, and thermodynamic stability in alkaline environments - Poor conductivity, potential surface oxidation during OER, thus reducing stability for long-term operation
Transition metal phosphides	TMPs	- Metallic or quasi-metallic conductivity, excellent HER/OER activity in both acidic and alkaline media due to tunable electronic structure, strong structural integrity with corrosion resistance in acidic/alkaline media - Surface oxidation to form oxides/phosphates decreasing conductivity and activity, synthesis challenges with the requirement of high temperature, toxic chemical sources, and specialized equipment

encapsulation of Cu within a carbon framework of the appropriate thickness. As a clear advantage, the encapsulated Cu cores distinctly retain their single-crystalline structure, as shown in HR-TEM, even after 60 days of exposure to ambient conditions.[95]

Additionally, they exhibit no XRD peaks for copper oxides, ensuring oxidation resistance. Another report marked further progress toward achieving improved chemical stability, a huge surface area, and high electrical conductivity through the development of core–shell FeCo@N–C spheres anchored within GNS.[96] Carbon shells protect the NPs against harsh environments, providing long-term stability, while FeCo NPs reduce the regional work function of the carbon surface, resulting in a synergistic effect that significantly enhances catalytic activity. A valuable report by Tu and coauthors designed ultrafine NiFe NPs with a small size encapsulated within a few-layered GNS

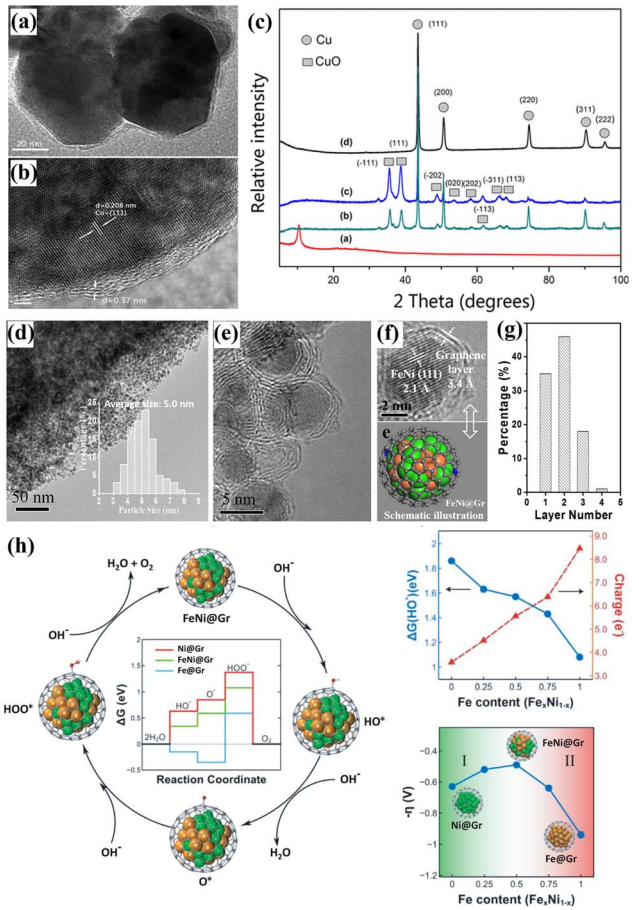

Fig. 3 (a and b) TEM images and (c) XRD pattern of the Cu encapsulated by GNS (reproduced from ref. 94 with permission from ACS, copyright 2018); (d) TEM image, (e and f) HR-TEM images, (g) schematic illustration of core–shell structure, (g) statistical analysis of the graphene layer number derived from FeNi NPs encapsulated by GNS, and (h) its specific electronic properties for enhancing catalytic activity towards OER (reproduced from ref. 97 with permission from Elsevier, copyright 2018).

with significantly high loading *via* a universal strategy (Fig. 3d–g).[97] In this research, the author examines and resolves issues, including large particle size, inhomogeneous distribution, incomplete encapsulation, and lower loading caused by high-temperature synthesis, by uniformly coating the dispersed NPs with a 3–5-layer thick GNS. The encapsulation of FeNi binary metal NPs within an ultrathin GNS layer can effectively modulate the electronic properties, leading to an enhanced catalytic activity towards OER (Fig. 3h).[97] In a further noteworthy study, Feng and coauthors fabricated a NiFe@N-GNS core–shell structure, utilizing N-doped GNS (NGNS) that offers enhanced electrical conductivity and a large surface area for retaining the NiFe core, thereby achieving superior electrochemical performance.[98] In another study, 3D N-GNS foam architectures incorporating Ge-QD@NGNS nanostructures have been reported for flexible energy storage applications.[39] In this configuration, 3–7 nm Ge QDs are encapsulated by self-supporting NGNS shells and uniformly anchored within the 3D foam. The interconnected porous framework ensures intimate contact between the Ge QDs and the conductive NGNS network, while an internal void of ~2.2 nm effectively buffers the volumetric expansion of Ge QDs during lithiation, thereby maintaining structural integrity and enhancing electrochemical performance. Furthermore, the open channels facilitate efficient electrolyte infiltration, while the robust yet flexible framework preserves high electrical conductivity, enabling rapid ion/electron transport and outstanding battery performance.

TMOs and TMHOs and their core–shell materials

TMO catalysts offer advantageous physicochemical properties, including superior theoretical specific capacities, durability, and cost-effectiveness, as well as abundance, making them a potential material for heterogeneous catalysis in various industrial chemical processes. Typically, the facile preparation of TMOs requires low temperatures; thus, they can be designed in various tailored sizes and morphologies. Despite their simplicity of synthesis and favorable activity for electrocatalysis, TMOs exhibit lower electrical conductivity and thus seek optimization in their electron transfer ability. In this context, defect engineering and plasma treatment are effective strategies to accelerate reaction kinetics, as opposed to their bulk counterparts.[99,100] TMOs are recognized as highly effective candidates for energy conversion and storage, resulting from their exciting catalytic behavior and exceptional capacities, as confirmed by theoretical studies. However, the long-term cycling operation often leads to large volume changes, which can cause breakdown (pulverization). As a result, the active material and the current collectors lose electrical contact, leading to a rapid loss of capacity over time. Furthermore, undesirable aggregation and leaching during cycling add up to activity/capacity decay.[38] To overcome these challenges, forming a core–shell structure with 2D carbons has emerged as an effective solution to enhance performance. A recent report by Zhang and coauthors indicates that coating the GNS layer on ternary Zn–Ni–Co oxide microspheres creates a synergistic effect that enhances conductivity, thermal/chemical stability, and mechanical strength.[101] It was discovered that GNS acts as an efficient 2D supporting substrate, retaining a uniform dispersion of the active material while shielding volume expansion, thereby offering excellent activity and longer cycling life. In another compelling investigation, Jin and coauthors designed a unique nanoarchitecture utilizing core–shell strategies, with 2D GNS serving as an electron collector. They covalently anchored a CoO core and a Co-doped g-C_3N_4 shell to create ample active sites, thereby delivering superior stability and catalytic activity towards ORR.[102] The synthesis of a porous hybrid structure derived from reduced graphene oxide (rGO) NSs uniformly attached with Fe_2O_3–MoO_3 NPs of approximately 8 nm was also reported.[103] The highly dispersed Fe_2O_3 provides additional active centers, improves contact with the matrix, and enhances stability, while also acting as pillars between GNS to form a porous architecture that facilitates catalytic activity while minimizing NPs detachment, thus enhancing charge transfer and improving activity with excellent stability (Fig. 4a–d). More recently, α-Fe_2O_3 nanoplates, consistently distributed and

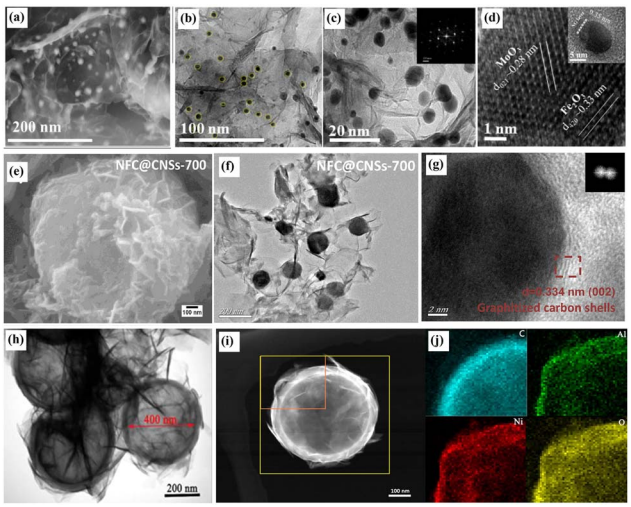

Fig. 4 (a) SEM image, (b and c) TEM images, and (d) HR-TEM image of rGO NSs uniformly attached Fe_2O_3–MoO_3 NPs (reproduced from ref. 103 with permission from Elsevier, copyright 2021); (e) SEM image, (f) TEM image, and (g) HR-TEM image of Ni–Fe–Co-based mixed metal/metal-oxides NPs confined within porous carbon nanosheets (reproduced from ref. 105 with permission from Elsevier, copyright 2021); (h) TEM image and (i and j) EDS analysis of C@Ni–Al LDH material[106] (reproduced from ref. 106 with permission from Springer, copyright 2019).

confined within the rGO network, were demonstrated to form a fluffy microstructure.[104] Interestingly, when rGO nanosheets are deliberately coated on another material's surface, they act as a barrier to block agglomeration and restacking of rGO sheets. In another study, a microsphere was formed by encapsulating hollow V_2O_5 on crumpled rGO, resulting in a 3D network with strong mechanical features, enhanced mass transfer, and reinforced structural stability. In an interesting study proposed by Yaseen and coauthors,[105] a 3D interconnected macro-porous framework of hierarchical flower-like morphology constituted uniformly dispersed Ni–Fe–Co-based mixed metal/metal-oxides NPs with a particle size of 50 nm confined within porous carbon nanosheets (Fig. 4e–g).[105] The developed material exhibits a meso- and macroporous structure that improves interfacial contact while mitigating the dissolution and accumulation associated with NPs, thus boosting stability and activity.

TMHOs are a highly desirable electrode material for energy storage applications. It offers several advantages, including high theoretical capacitance, cost-effectiveness, compositional flexibility, and eco-friendliness. For TMHOs, the major drawbacks are low conductivity, agglomeration, and volume expansion, which significantly hinder their ability to reach optimum performance.

To address these limitations and achieve high power and energy densities, novel architectural designs are needed to enhance intrinsic features. In a recent report, GNS encapsulated spheric structures of homogenously dispersed C@Ni–Al LDH were pronounced (Fig. 4h–j).[106] This was confirmed by the regular dispersion of GNS on C@Ni–Al LDH spheres, which exhibit the role of spacers in blocking the restacking of GNS, thereby ensuring mechanical integrity and improved electrical conductivity. A flower-like structure of $Ni^{2+}/Mn^{2+}/Al^{3+}$ LDH@N-GNS hybrids coating on nickel foam was reported.[107] In addition, Chen and coauthors also developed a specific architecture derived from Ni–Mn LDH-coated carbon attached on nickel foam.[108] Such interesting 3D configurations have proven beneficial in achieving an optimum mass diffusion rate and rapid transfer pathway, thereby enabling high electrochemical performance. A study by Markovic and coauthors revealed that the catalytic activity of the TMHO series follows the trend Mn < Fe < Co < Ni. This behavior could be attributed to a decrease in the strength of OH_{ad}–$M^{2+\delta}$, with Mn–OH being the strongest and Ni–OH being the weakest.[109] Additionally, the combination of multiple TMHOs can create various active sites, leading to an overall enhancement of catalytic activity.[110,111] As a general trend, encapsulating TMOs and TMHOs within 2D carbon materials improves electrochemical reaction kinetics by preventing the agglomeration/leaching of active metals, enhancing overall conductivity and activity, and accommodating volume changes during cycling.

TMSs and their core–shell structure by 2D carbon materials

Transition metal sulfides (TMSs) are extensively studied for many industrial applications, including hydrodesulfurization, CO_2 reduction, and energy storage/conversions. In recent years, their potential in energy storage has attracted growing attention, owing to their distinctive characteristics that enhance catalytic efficiency. Among them, layered TMSs are the most widely explored. The rationale behind their intensive research includes lower volume expansion during lithiation and superior rate capacity and cycling ability as compared to TMOs.[112] When studying catalytic mechanisms involving layered TMSs, the catalytically active sites were identified as 1D edge sites of the layered structure.[113] The recent success of TMSs in electrocatalysis has spurred increased research efforts into specifically layered TMSs as promising active and inexpensive catalysts. Despite their high theoretical capacities compared to TMOs and TMHOs, this potential class of nanomaterials suffers from cracking, fracture, and particle isolation during volume changes during cycling, resulting in insufficient cycle stability and rate capability in electrocatalysis. Li and coauthors introduced the controllable fabrication of N,S-doped GNS encapsulating cobalt-rich sulfides (Co_8FeS_8@NSGNS)-based hybrid (Fig. 5a–e).[114] The uniform distribution of Co_8FeS_8 NPs and an encapsulated structure greatly promoted electron transfer, which effectively optimizes the electronic structure to enhance the ORR activity (Fig. 5f). In this context, Qiu and coauthors have tried to address those issues using a novel nanostructure based on CoS_2 spheres confined by N-GNS.[115] The fabricated CoS_2@N-GNS exhibited spherical structures with diameters ranging from 1.5 to 2 μm and a narrow particle size distribution. These spheres were uniformly wrapped by N-GNS, resulting in crinkled, rough surfaces attributed to the presence of flexible and ultrathin N-GNS layers. Such a mesoporous structure can increase electron transfer, reactivity, and create a short ion/electron diffusion pathway while minimizing volume changes and suppressing interfacial reaction. The outstanding

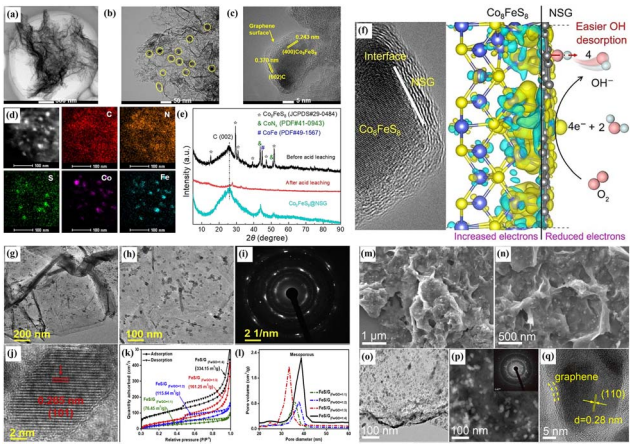

Fig. 5 Morphology, structure, and composition analysis based on (a) TEM, (b and c) HR-TEM, (d) EDS, and (e) XRD characterizations for the Co_8FeS_8@NSGNS; (f) effect of core–shell Co_8FeS_8@NSGNS towards electronic properties for enhancing catalytic properties (reproduced from ref. 114 with permission from Elsevier, copyright 2024); (g and h) TEM images, (i) SAED analysis, (j) HR-TEM image, and (k and l) N_2 adsorption–desorption isotherm measurement for the Fe sulfide/rGO hybrid (reproduced from ref. 117 with permission from Elsevier, copyright 2019); (m and n) SEM, (o and p) TEM, (q) HR-TEM images of Ni–V sulfide NPs encapsulated on GNS (reproduced from ref. 118 with permission from RSC, copyright 2024).

electrochemical performance was also demonstrated by Co sulfide NPs (average size ~150 nm) uniformly wrapped by or anchored onto GNS, as reported by Huang and coauthors.[116] More recently, a distinct nanostructure consisting of Co sulfide nanocages coated within GNS has been developed.[34] The analysis of the synthesized material reveals that it contains hollow, uniform CoS_2 nanocages measuring 50–80 nm in diameter and with 15–25 nm thick wall. These nanocages are then encased within GNS to create a sandwiched configuration, which effectively prevents the undesirable restacking of GNS, thereby facilitating rapid mass diffusion. Gautam and coauthors synthesized Fe sulfide/rGO hybrid, which shows the uniform distribution of the FeS NPs (~5–10 nm) homogeneously embedded on the surface of rGO sheet (Fig. 5g–j). The N_2 adsorption–desorption suggests the mesoporous features of such hybrid with the large surface area of (334.15 m^2g^{-1}) (Fig. 5k–l), highly beneficial to provide rich active sites, various ion/charge transfer pathways, and reactant diffusion channels for improving catalytic performance.[117]

Tao and coauthors revealed a hierarchical structure of CoS_2@GNS, where CoS_2 NPs were tightly encapsulated within a thin GNS layer to result in a synergistic effect, helping to buffer the volume changes that CoS_2 undergoes during cycling and also improving the electron/ion transfer, resulting in excellent electrochemical activity over time.[119] In another study, the development of Co–Fe sulfides well-anchored within mesoporous N–C was reported. The uniform distribution of Fe positively affects the initial steps of the catalytic process, *i.e.*, adsorption and activation of O-containing items, while the strong connection of the Co–Fe–S NPs and carbon enhances the overall stability and efficiency by promoting electron and ion transfer.[120] Guo and coauthors introduced a hierarchical structure of Ni–V sulfide NPs encapsulated on GNS.[118] TEM analysis shows Ni–V–S NPs with an average size of approximately 20–30 nm attached to GNS (Fig. 5m–q). The interconnection of GNS coating Ni–V–S NPs efficiently decreases the ion diffusion route among the electrolyte and electrode, thereby boosting electrochemical behaviors, significantly potential in energy storage applications. In a recent study, Guo and coauthors achieved uniform encapsulation of high-quality Co_2CuS_4 in N-GNS.[121] The SEM and TEM analysis indicate that N-GNS is uniformly wrapped with Co_2CuS_4 NPs with a typical size of ~21 nm. As a result, the nanomaterial exhibits a high specific surface area and excellent conductivity, which prevents accumulation while maintaining nanoparticle morphology, thereby enhancing its efficiency.

TMCs and their core–shell structure by 2D-carbon materials

TMCs are a type of interstitial alloy where carbon atoms are placed into the interstitial sites of the TM crystal. The three primary types of atomic interactions involved in the synthesis of TMCs are covalent bonds (shared electrons), ionic bonds (electron transfer), and metallic bonds (electrons holding metal atoms together).[122] These compounds exhibit high melting points, exceptional conductivity, and favorable physical properties, crucial for catalytic processes.[123] In addition, this class of materials has high anticorrosion ability in harsh conditions.[124] Owing to the promising potential of TMCs, ongoing research continues to explore their synthesis with tailored morphologies and properties, aiming to unlock applications across diverse fields of energy storage and conversion applications.[125,126] TMCs show great potential as earth-abundant, promising alternatives to expensive platinum-metal-based catalysts due to their Pt-like activity. However, TMCs require further in-depth research and development to overcome the drawbacks associated with these materials before they can be widely commercialized. In this respect, various strategies are being implemented to achieve higher efficiency and reliability, including tunable nanoarchitecture, which enhances the interaction between the conducting support and the active material to achieve an optimal binding energy for the reaction and sufficient active sites. Specifically, a reduction in particle size has proved to be an effective approach to achieve higher electrochemical performance. In this context, constructing core–shell TMCs@carbon nanostructures not only enables the controlled production of small NPs but also significantly enhances the communication between the active catalysts and their 2D support. Zhang and coauthors reported designing ultrasmall TMC NPs encapsulated in N,S-doped GNS as precious metal-free electrocatalysts for HER,[127] in which a high density of MoC_x (≈2.8 nm) NPs is encapsulated in a porous N,S-GNS matrix (Fig. 6a–e). The structure and composition of the developed catalyst were well analyzed by powder XRD and XPS (Fig. 6f–i). In another case, Li and coauthors developed a hybrid containing Mo_2C coated by N,P–C layer, which appears to have rough and wrinkled under SEM and TEM imaging.[128] The Mo_2C NPs are uniformly distributed with an average particle size (dia: 2–5 nm) with

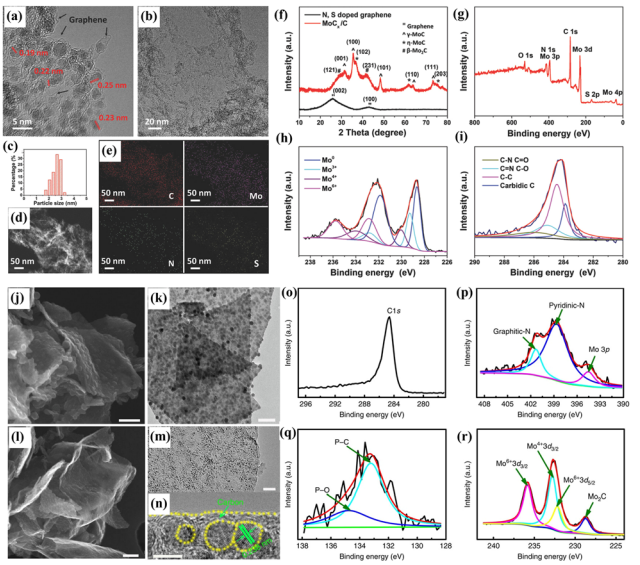

Fig. 6 (aand b) TEM, (c) size distribution, (d and e) TEM-EDS color mapping, (f and i) XPS analysis for the MoC_x NPs encapsulated in a porous N,S-GNS (reproduced from ref. 127 with permission from Wiley, copyright 2018); (j–n) SEM and TEM images, (o–r) XPS analysis for the hybrid of Mo_2C coated by N,P–C layer (reproduced from ref. 128 with permission from Springer, copyright 2016).

a high density and strong interaction with carbon shells, thereby preventing aggregation (Fig. 6j–n). The XPS study effectively elucidated the valence states of the components in the hybrid structure, as well as its composition (Fig. 6o–r). Interestingly, the unique, enriched microporous structure of the as-fabricated hybrid material offers an enhancement in both electrolyte penetration and charge transfer abilities. In another aspect, previous reports have indicated that incorporating N–C cages with TMs into a single, regular nanoarchitecture could significantly enhance the catalytic behavior of the catalyst product. A report on the fabrication of Co_3ZnC/Co nano-heterojunctions indicates the formation of NPs with a particle size of approximately 10–30 nm, encapsulated by 3–5 N-GNS layers, uniformly assembled into spherical architectures with an average diameter of approximately 900 nm.[129] This offers protection against corrosion and aggregation of NPs, ultimately providing ample active sites for enhanced catalytic activity and stability.

In a recent investigation by Liu and coauthors, they developed electrocatalysts consisting of ultrasmall Mo_2C nanoparticles with an average particle size of approximately 3.6 nm, embedded within 2–4 sheets of N-doped carbon structure, which was realized through the deliberate engineering of active sites.[130] The ability of Mo_2C to act as a charge donor while N species act as charge acceptors creates a synergistic response to generate superactive non-metallic catalytic sites within carbon layers. Such a mechanism enables the hybrid material to achieve excellent electrochemical HER performance in a universal pH medium. Liu and coauthors,[131] reported a distinctive Fe_3C@Fe/N-doped GNS catalyst, exhibiting a silk veil-like morphology with Fe_3C NPs encapsulated within GNS. Furthermore, a mesoporous architecture featuring uniformly distributed Fe_3C NPs embedded in GNS layers was also designed by Jiang and coauthors,[132] in which small Fe_3C NPs were effectively dispersed on N-GNS, offering them strong chemical stability. The synergistic behavior was observed due to the activation effect of Fe_3C NPs on carbon layers, as well as C-N_x active sites, leading to excellent electrochemical properties. In a continued pursuit, Yang and coauthors fabricated MoC_x NPs with a small particle size of approximately 16.5 nm, uniformly encapsulated within N-GNS, forming a robust superstructure in which the graphene layers effectively prevent surface oxidation and stabilize the hybrid during catalytic reactions.[133] Various TMCs@carbon hybrids with distinct nanostructure and tailored physicochemical features have also been recognized as effective nonprecious metal-based catalysts.[134–137]

TMNs and their core–shell structure by 2D carbon materials

TMNs, a class of materials with low nitrogen content, exhibit superconducting behavior, higher refractoriness, and enhanced hardness properties.[138–140] The above physicochemical properties make them an ideal choice for a wide range of applications. Besides TMC, these materials have the potential to replace platinum-group metals due to their "platinum-like" behavior. The formation of carbide and nitride undergoes electronic modulation, specifically in the d-band, which influences their catalytic activity. Although various structures of TMNs have been explored, TMNs still offer significant potential for further study, particularly in comparison to TMOs and TMHOs materials. In the current state, a new potential class of 2D TMCs and TMNs has garnered noteworthy attention due to their extraordinary electrochemical properties, specifically MXenes.[141] They offer various advantages, including higher electrical conductivity, hydrophilicity, making them an ideal choice for electrochemical applications. As discussed earlier, TMNs have been shown to possess superior properties compared to other alternatives; therefore, they are a favorable class for electrochemical reactions. Although TMNs have emerged as important multifunctional nanocatalysts with well-known properties, integrating them with carbon materials to form effective nanoarchitectures further enhances their prospective functionalities and usage. Regarding this, an advanced electrocatalyst featuring FeN with a particle size of ~10 nm, anchored on N-GNS with a thickness of $\sim 3 \pm 0.2$ nm, was reported.[142] The hybrid material achieved excellent performance in solar cell applications due to its strong interactions among the constituent materials and the blockage of the core FeN NPs agglomeration. Further reports contributed an important step forward in enhancing the properties of core–shell FeN@NGNS by fabricating an aerogel.[143] The construction of 3D networks maximizes the synergistic benefits of integrating GNS with FeN. Uniformly dispersed FeN NPs (5–20 nm) across the extensive GNS surface prevent agglomeration, offering abundant active sites, shortened mass diffusion pathways, and superior charge transfer, thereby delivering markedly enhanced performance than the simple FeN/NGNS mixture. Lately, Li and coauthors have successfully designed a GNS-encapsulated TMNs

($Fe_xMn_{6-x}Co_4$-N@C), which allowed precise control over the resulting hybrid material.[144] The porous structures, uniformly encapsulated by GNS, offer protection against harsh conditions and thereby extend the stability of the electrocatalysts. A distinctive 3D structure, consisting of intertwined mesoporous VN nanowires encapsulated by N-doped carbon layers and assembled into a self-supported film, has been reported.[145] In this respect, the synergistic effect brought about by VN nanowires and an N-doped carbon shell offers desirable capacitive performance, featuring a 3D porous network and excellent conductive properties due to the accessible active sites at VN nanowires, which facilitate higher charge storage and chemical stability from the carbon shell, thereby resisting the leaching of active VN nanowires during operation. Chen and coauthors reported the fabrication of an N-GNS encapsulating Fe nitride (Fe_2N@NC) electrocatalyst to explore the influence of the interaction of Fe_2N and N-GNS on the catalytic activity.[146] The TEM image shows that the Fe_2N NPs with an average size of approximately 50 nm are uniformly dispersed on the wrinkle-rich N-GNS (Fig. 7a–d). The structural analysis of the developed catalyst, conducted *via* XRD, XPS, and DFT studies, confirms the charge density redistribution in Fe_2N@N-GNS, resulting from the formation of charge-deficient Fe due to distinct charge transfer from Fe to N-GNS, thereby enhancing its catalytic activity towards the conversion of nitrate to ammonia (Fig. 7e–h).

Shu and coauthors introduced a unique worm-like architecture of hierarchically porous N-rGO embedded with $Co_{5.47}N$ NPs (Fig. 7i–r).[147] Advantaging from the special worm-like configuration to expose rich active centers, the close contact between $Co_{5.47}N$ NPs and N-rGO, and the modified electronic structure of the $Co_{5.47}N$ due to strong interaction between catalyst and substrate, the $Co_{5.47}N$@N-rGO displays outstanding bifunctional catalytic activities. A novel 3D hybrid in which $Co_{547}N$ NPs were encapsulated within N-carbon was also reported, featuring a dodecahedral-like morphology with a rough and shrunken surface due to its porous structure. This polyhedral structure ensures strong interfacial contact between $Co_{5.47}N$ and the carbon matrix, encapsulated with 3–5-layer thick graphitic shell, thereby enhancing the catalyst's stability.

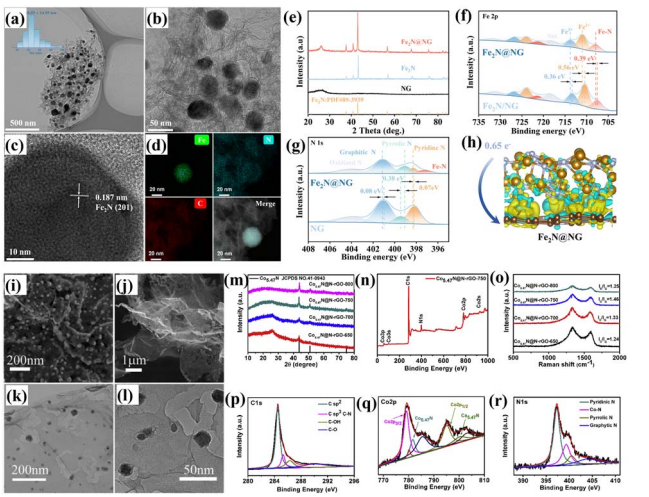

Fig. 7 (a and b) TEM, (c) HR-TEM, (d) EDS mapping, (e–g) XPS analysis, and (h) electronic properties of N-GNS encapsulating Fe nitride (Fe_2N@NC) (reproduced from ref. 146 with permission from RSC, copyright 2025); (i and j) SEM, (k and l) TEM, (m) XRD patterns, (n) Survey XPS spectrum, (o) Raman spectra, (p–r) High resolution XPS spectra for porous N-rGO embedded with $Co_{5.47}N$ NPs (reproduced from ref. 147 with permission from Elsevier, copyright 2020).

TMPs with their core–shell structure by 2D carbon materials

TMPs possess an anisotropic crystal structure, where metal atoms are arranged in a triangular prismatic fashion, with phosphide atoms surrounding them. This arrangement results in a large number of unsaturated surface atoms that favor specific properties. Interestingly, metal and phosphorus (P) atoms are capable of acting like functional centers,[148,149] with a true active center within this class of material being *in situ* generated surface oxy/hydroxides and phosphates. At the same time, phosphides promote rapid charge transfer owing to their high electrical conductivity, surpassing their counterparts.[150] TMPs exhibit greater electrocatalytic stability than TMNs.[140] TMPs as electrocatalysts have gained significant attention for multiple electrochemical applications, and their catalytic behavior generally surpasses that of the corresponding TMSs, primarily due to their superior capability towards hydrogen adsorption.[151] To further enhance the performance of such TMPs in harsh environments, hybridizing these NPs with 2D carbon layers is a promising strategy. This hybrid material creates a synergistic effect, with carbon acting as a protective cage that neutralizes non-metal elements, resulting in enhanced chemical stability. One such finding by Pu and coauthors, synthesized FeP NPs confined by N,P–C sheets.[152] Analytical analysis demonstrated the homogeneous distribution of FeP NPs within carbon layers, promoting high electronic conductivity, high anticorrosion in the electrolyte, and preventing agglomeration. Wang and coauthors reported an advanced catalyst with FeP NPs embedded in N,P–C layers of microporous carbon nanofibers achieved by electrospinning.[153] The active catalyst is available in the form of well-defined NPs encapsulated in the N,P–C shell having a thickness of around 6.5 nm (Fig. 8a–d). The structure indicates a microporous structure with large specific surface area (Fig. 8e), beneficial for more stable active sites to increase electrocatalytic performance. Zhuang and coauthors synthesized uniformly dispersed Co_2P NPs encapsulated within wrinkled N, P-doped GNS,[154] which exhibits Co_2P NPs (30 ± 5 nm in diameter) dispersed both within and partly outside the GNS structure without aggregation. Furthermore, it has been demonstrated that utilizing 3D carbon with heteroatom doping, specifically N and P, can enhance the electrochemical activity and corrosion resistance in harsh electrolyte media. The enhancement stems from the creation of catalytically active sites and the synergistic behavior of constituent atoms. Yang and coauthors designed a porous carbon sandwich configuration containing 0D Co_2P@C NPs dual-doped with N and P,[155] which demonstrated a synergistic effect responsible for improving charge transfer, mass diffusion, and providing ample active sites. The possible

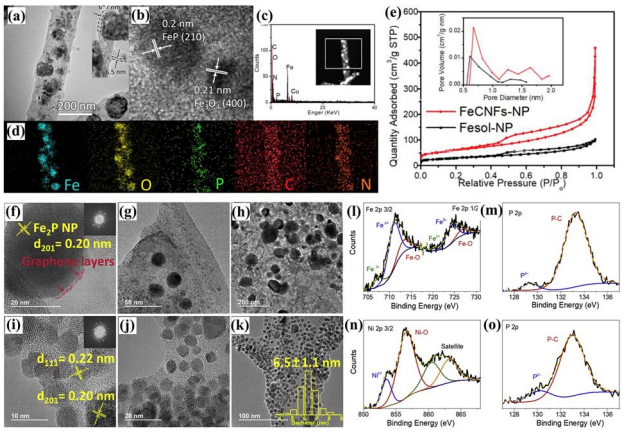

Fig. 8 (a) TEM, (b) HR-TEM, (c and d) EDS analysis, and (e) BET measurement of the FeP NPs embedded in N,P–C layers (reproduced from ref. 153 with permission from Elsevier, copyright 2019); TEM images of (f–h) FeP/N-GNS and (i–k) NiP/N-GNS, and (l–o) their XPS analysis (reproduced from ref. 157 with permission from Cell Press, copyright 2022).

explanation for higher HER performance can be attributed to Co_2P and N, P dopants that specifically enhance the free adsorption energy towards hydrogen. Another 3D porous network derived from N-doped carbon-confined Co_2P nanoparticles was reported to offer significant advantages, including abundant active centers and improved charge/ion transfer rates and distances.[156] In subsequent research, a Cu3P coverage by porous N,P–C was designed to create a 3D hierarchical porous morphology with homogeneous tiny Cu NPs and a high specific surface area. Overall, these unique nanoarchitectures offer several advantages, including ample active sites and rapid reaction kinetics, as well as smooth transportation of reactants and products.

Zhang and coauthors[158] reported a novel hybrid structure combining TMC and TMP nanostructures (*e.g.*, MoP and Mo_2C) encapsulated within N-doped graphitic carbon shells. This architecture enables the achievement of narrow particle sizes (~4–10 nm) for the MoP/Mo_2C@C NPs, which are coated with graphitic carbon nanolayers, thereby preventing the aggregation of anchored NPs and ensuring favorable durability during electrochemical reactions over a wide pH range. Hu and coauthors developed a method for synthesizing Ni_2P, Fe_2P, and FeP supported by N-GNS.[157] TEM analysis indicates Ni_2P NPs homogeneously dispersed with an average diameter of 6.5 ± 1.1 nm, while Fe_2P and FeP NPs appear to have a much wider distribution of size, ranging from 20 to 200 nm (Fig. 8f–k). The surface chemical analysis investigated by XPS shows a strong interaction between the metal phosphides and N-GNS (Fig. 8l–o), resulting in outperformance in terms of activity and stability for catalytic reactions.

Synthesis methods of core–shell catalyst derived from carbon material

The core-sell hybrids are an emerging class of nanostructures, where TM clusters are fully encapsulated by few-layer graphitic carbon nanosheets, providing improved activity and stability. The 2D carbon layers can anchor, homogenously dispersing, along with the stabilization of active metal within their structure.[159,160] The surface electronic states are tunable through precise changes in the geometric parameters of metal nanoparticles, thereby affecting both the local strain and the atomic coordination number on their surface. In addition, these materials exhibit special interactions between core and shell components, along with facilitated charge and mass transport.[39,161] To achieve optimal catalytic performance from the outer carbon surface, the charges of TMs can enter the graphitic shell, while the graphitic carbon can prevent the reactant and electrolyte from physically contacting TMs in order to provide chemical stability in harsh conditions. Therefore, precise control over the core–shell hybrid structure *via* tailored strategies is essential to modulate the properties and thereby enhance the performance of the resulting materials.

Hydrothermal and solvothermal methods

Hydrothermal/solvothermal reactions have been widely accepted as a synthesis technique for fabricating TM@carbon materials. This is due to their various advantages, including simplicity in operations, robustness, inexpensiveness, and scalability. In this context, Qiu and coauthors designed CoS_2@N-doped GNS using a simple and non-templated solvothermal approach.[115] Typically, CoS_2 spheres were synthesized *via* a hydrothermal method at 160 °C for 24 h in a solution containing $CoCl_2 \cdot 6H_2O$ and $Na_2S_2O_3 \cdot 5H_2O$. The resulting CoS_2 was subsequently treated with $(NH_4)_2S_2O_8$ and then combined with GO and other reagents under stirring for 2 h, followed by heating at 150 °C for 4 h. In a separate report of interest, a hydrothermal reaction at 200 °C during 12 h is employed to synthesize a hierarchical GNS-encapsulated CoS2 hybrid using a homogeneous solution comprising GO, $Co(OAc)_2$, and $Na_2S_2O_3 \cdot 5H_2O$.[119] Research from Liang and coauthors[33] introduced a two-step hydrothermal process of Co_3O_4 NPs uniformly coated within N-GNS to form a hybrid structure. Initially, $(Co(OAc)_2)$ underwent a stepwise synthesis of hydrolysis and oxidation at 80 °C to achieve Co_3O_4 NPs anchored to GO. In the subsequent step of hydrothermal at 150 °C, the Co_3O_4 crystallization as well as GO reduction is achieved. A facile impregnation–solvothermal approach for fabricating mesoporous rGO microspheres reported by Xu and coauthors[162] revealed that uniformly dispersed Fe_2O_3 NPs were effectively encapsulated by graphene sheets. The fabrication process involves the preparation of a homogeneous dispersion comprising rGO and Fe(NO3) 3·9H2O, which is then suffered a thermal treatment at 353 K for 8 hours. Another study proposed a hybrid material with interconnected 3D Fe_2O_3 NPs confined by GO sheets, prepared by heat treatment of urea, $Fe(NO_3)_3$, and GO mixture for 8 h in hydrothermal conditions. In the next step, the as-prepared mixture is freeze-dried at low temperature and pressure during 24 h.[163] Wang and coauthors[164] recently reported 3D β-$Ni(OH)_2$ spheres encapsulated within GNS. After the hydrothermal process of $NiCl_2$ and PSS solution (pH = 11) at 180 °C for 6 h, β-$Ni(OH)_2$ was as-prepared. It then suffered

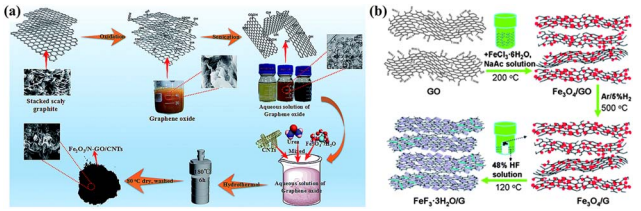

Fig. 9 (a) A hydrothermal process for the synthesis of 3D Fe_2O_3/N-GN/CNTs hybrid[165] (Copyright from RSC); (b) a hydrothermal process for the synthesis of FeF_3/GNS (reproduced from ref. 166 with permission from RSC, copyright 2013).

a solvothermal reaction at 180 °C during 12 h in the presence of PLL, EG, and GO to get the encapsulation structure. Zhou and coauthors introduced the formation process of the Fe_2O_3/N-GN/CNTs hybrids prepared by a simple solvothermal route (Fig. 9a).[165] First, GO synthesized by a modified Hummers' method was mixed with GO, CNTs, and Fe^{2+} cations to achieve a uniform solution, in which the functionalized surface of the GO sheets anchored Fe^{2+} *via* electrostatic interactions. After that, the solution was added with urea under vigorous stirring condition, followed by hydrothermal treatment at 180 °C for 6 h to produce 3D Fe_2O_3/N-GN/CNTs hybrid. Ma and coauthors introduced the fabrication procedure of GNS-wrapped FeF_3 nanocrystals, in which Fe_3O_4/GO composite was initially fabricated *via* a solvothermal method based on starting materials of GO, NaAc, and $FeCl_3 \cdot 6H_2O$, followed by annealing at 500 °C for 2 h under Ar/H_2 gas to convert into Fe_3O_4/GNS (Fig. 9b).[166] Finally, the Fe_3O_4/GNS powder was heat-treated with HF at 120° to achieve $FeF_3 \cdot 3H_2O$/G and then 200 °C for 4 h in an Ar atmosphere to produce the final product of FeF_3/GNS. Recently, Co_2CuS_4@N-GNS was successfully synthesized through a solvothermal reaction at 180 °C for 6 h with the use of a solution containing GO, $Cu(NO_3)_2$, $Co(NO_3)_2$, and CH_4N_2S.[167] Several studies have also demonstrated the employment of the hydrothermal process to prepare core–shell hybrids. Notable examples include Co sulfides@GNS by Huang and coauthors,[116] Fe_2O_3@NGNS by Yang and coauthors,[37] α-Fe_2O_3 nanoplates@rGO by Quan and coauthors,[104] and $Ni^{2+}/Mn^{2+}/Al^{3+}$ layered triple hydroxide@NGNS hybrids by Ishaq and coauthors.[107] The challenges associated with the above-discussed techniques for developing high-quality hybrid materials include the use of surfactants, organic solvents, and stabilizers. Thus, to ensure optimal interaction between TM catalysts and 2D carbon support, these techniques could be combined with post-annealing treatment. Several reports have demonstrated the successful synthesis of hybrid materials. Gue and coauthors performed a solvothermal reaction involving $CoCl_2 \cdot 6H_2O$, CH_4N_2S, EG, and GO for 24 h, maintained at 160 °C. To achieve GNS wrapped monodispersed CoS_2 nanocages, the product from the initial step was subjected to annealing in Ar at 400 °C during 5 h.[34]

In another study, a Co@CoO_x material coated with a graphitic layer was designed using a hydrothermal and subsequent post-annealing process.[87] Specifically, the Co-EDTA complex achieved by a solution of NaOH, $Co(NO_3)_2$, and Na_2EDTA was treated in a hydrothermal vessel for 24 h at 200 °C. Finally, this Co-EDTA complex was heat-treated for 2 h in H_2 to produce Co@CoO_x@C solid.

Thermal treatment methods

Thermal synthesis has proven to be an effective approach for deliberately achieving core–shell catalyst@carbon hybrids. The application of thermal energy can transform reaction precursors into desirable hybrid materials. Nevertheless, the limited morphological control of TMs nanostructures' distribution, as well as their size, needs to be addressed and could be overcome through doping, using specific chemicals and processes. In this context, a Co@CN hybrid structure through calcination of Co-MOF, as well as ZIF-67 in an inert argon atmosphere, was proposed by Zhong and coauthors at 800 °C during 8 h.[168] Wang and coauthors prepared the catalyst through a three-step method, in which PAN/Fe CNFs were initially prepared by the electrospinning technique (Fig. 10a).[153] After that, N-CNFs depositing Fe_3O_4 NPs were achieved by an oxidative stabilization step at 240 °C, followed by a carbonization process at 800 °C. Finally, an annealing step in N_2 in the presence of NaH_2PO_2 source was applied at 350 °C to produce FeP NPs in a final product. Meanwhile, Wu and coauthors successfully fabricated GNS encapsulating 3d TM NPs (Ni, Co, Fe@GNS) through a pyrolysis process (Fig. 10b).[169] In a typical process, $Ni(NO_3)_2 \cdot 6H_2O$ and NaOH was dissolved in water to form two solutions, which were then mixed to result in green precipitate of $Ni(OH)_2$. Then, Ni(OH)2 and citric acid were dissolved in water to form a solution, followed by drying at 110 °C in air for 12 hours. After that, the sample was placed in a furnace under a N2 atmosphere for thermal treatment at high temperatures to achieve the Ni@GNS material. Hu and coauthors prepared Fe/Ni phosphides confined porous 3D GNS *via* a simple and scalable preparation procedure (Fig. 10c).[157] In brief, Fe^{2+} or Ni^{2+} salts were dissolved in an aqueous chitosan solution, followed by a subsequent precipitation step in NaOH solution to create hydrogel microspheres, which were impregnated with P_4O_{10}. After drying the sample, a pyrolysis step was performed to produce metal phosphides grafted on porous 3D NGNS. Wang and coauthors reported N,P–C-anchored Cu phosphide NPs. The synthesis process involves the self-assembly of Cu^{2+} in the presence of linkers to synthesize Cu-NP MOF, which is then subjected to carbonization and phosphidation as a further step to achieve a Cu NPs confined N, P-doped carbon layer.[170] Mo_2C coated within N,P–C shells and integrated with rGO codoped with N and P was developed by Li and coauthors.[128] The hybrid was synthesized by annealing PMo_{12}–PPy/rGO under N_2 flow at 900 °C during 2 h, followed by treatment with 0.5 M H_2SO_4 to remove unnecessary species. A simple strategy to prepare Co NPs encapsulated by NGNS *via* annealing in Ar for the colloids of Co-based Prussian blue at 400–900 °C.[171] Balamurugan and coauthors developed FeN@NGNS hybrids by pyrolyzing in Ar for CH_2N_2, $FeCl_3 \cdot 6H_2O$, and GO at 900 °C during 150 min. After that, the resulting material was treated by H_2SO_4 solution, washed with water and ethanol, followed by drying during 6 h at 60 °C.[142,172] Cui and coauthors proposed a facile two-step

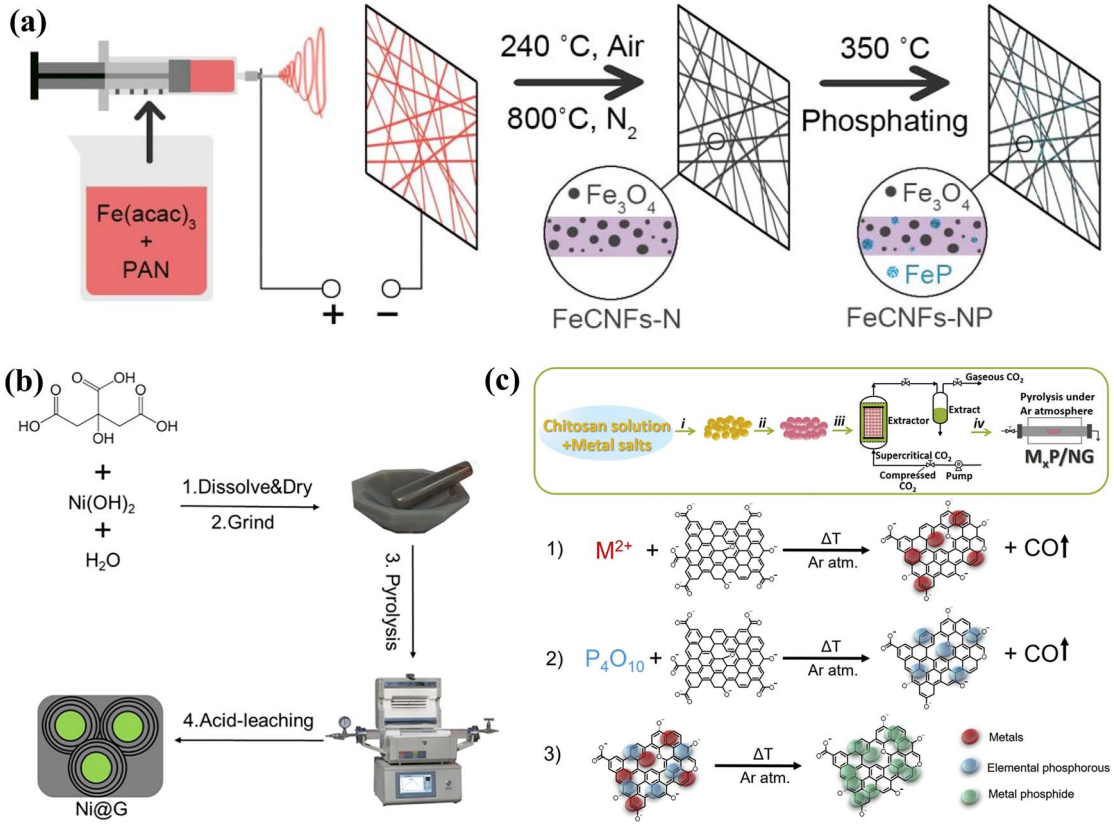

Fig. 10 (a) Schematic illustration for the fabrication of Fe oxide and phosphide encapsulated within N,P-doped microporous carbon nanofibers *via* a three-step method (reproduced from ref. 153 with permission from Elsevier, copyright 2019); (b) schematic procedure for the synthesis of Ni@GNS (reproduced from ref. 169 with permission from Elsevier, copyright 2022); (c) preparation procedure of metal phosphides-anchored 3D N-GNS and formation mechanism (reproduced from ref. 157 with permission from Cell Press, copyright 2022).

strategy to prepare catalyst of FeO_x encapsulated within NGNS-C, which involved pyrolyzing a Fe precursor and phenanthroline at high temperatures for 120 min in the presence of Ar gas, followed by treatment with HCl to eliminate unnecessary species.[173]

A report by Zhang and coauthors describes the design of MoP and Mo_2C NPs coated within a few-layered N-carbon.[158] The synthesis procedure involves heating a solution of P_4Mo_6 and DCA in water at 100 °C to achieve dissolution, followed by drying to collect the powder material. Finally, the as-obtained powder material was subjected to stepwise annealing at 500 °C for half an hour, followed by annealing at a high temperature for 6 h. A core–shell structure of bimetallic TMs coated by GNS has been reported for the NiFe@N-GNS system, which involves the preparation of NiFe-Prussian blue analogues (PBA) through co-precipitation, then this gel-like precursor was subjected to annealing at 700 °C. This allows the CN-linkers in precursor PBA, to *in situ* transform at higher temperature and inert Argon atmosphere into NGNS layers along with the reduction of Ni and Fe metals to NiFe alloy NPs. Recently, Su and coauthors reported a zero-dimensional Co_3ZnC/Co confined by N-NS, prepared by thermal treatment of PBA under a nitrogen atmosphere at high temperatures for 4 h.[129] The thermal synthesis process has been widely applied to fabricate diverse core–shell hybrids based on TMs and 2D carbon layer materials.[86,154,174–177]

Other methods

In addition to the aforementioned hydrothermal and thermal processes, several other approaches have also been developed to fabricate core–shell hybrids for various widespread purposes. Yang and coauthors proposed a co-assembly strategy for preparing Co_3O_4 confined within GNS. Here, the oxide NPs (Co_3O_4 NPs) are grafted with aminopropyltrimethoxysilane to impart a positive charge. Then, the electrostatic force between the negatively charged GO and the positively charged NPs undergoes assembly. Finally, chemical reduction is performed.[38] In this manner, the as-obtained hybrid material prevents the agglomeration of NPs and offers various advantages, including excellent conductivity and good controllability of volume during the reaction. Liu and coauthor introduced a laser synthesis procedure (Fig. 11a),[178] in which chlorides of Cr, Mn, Fe, Co, and Ni with the same molar ratios were dispersed in water to form a homogeneous solution. After that, the solution was coated on the LIG-coated carbon paper, followed by drying at 80 °C for 30 min in a vacuum oven. Finally, the sample was subjected to laser irradiation with the employment of Nd: YAG laser having a wavelength of 1064 nm in Ar at a scanning rate of 2000 mm s^{-1} to achieve the final product of GNS shell encapsulated high-entropy alloy NPs. Hang and coauthors developed a robust approach to produce 3D Zn–Ni–

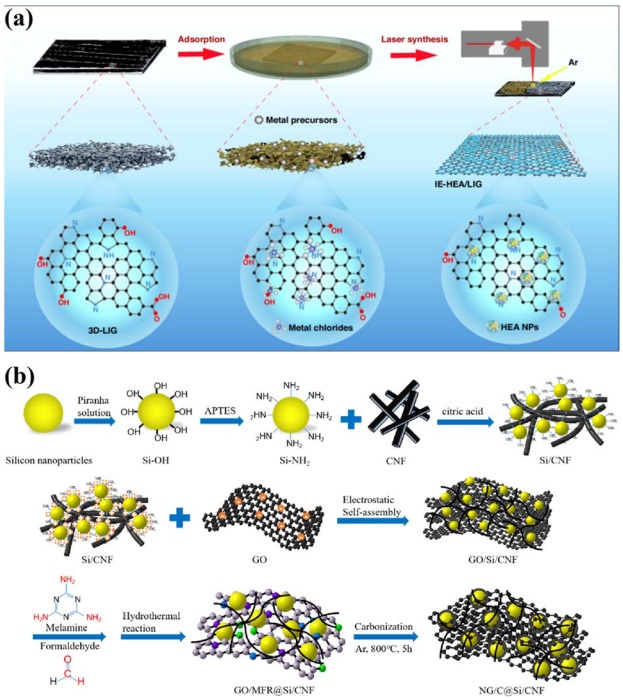

Fig. 11 (a) A laser solid-phase synthesis route for the fabrication of GNS shell encapsulated high-entropy alloy NPs (reproduced from ref. 178 with permission from Springer, copyright 2024); (b) schematic diagram for the synthesis process of NGNS/C@Si/CNF hybrid material (reproduced from ref. 180 with permission from Springer, copyright 2022).

Co oxide coated by GNS.[179] Regarding this, the ternary oxide was initially synthesized through a chemical reaction between $Zn(NO_3)_2$, $Ni(NO_3)_2$, and $Co(NO_3)_2$, followed by an annealing step. The resulting core–shell hybrids were fabricated through electrostatic assembly between PAH-modified Zn–Ni–Co oxide and GO, followed by treatment with N_2H_4. Aadil and coauthors reported an α-Fe_2O_3 entangled rGO layer prepared by a facile ultra-sonication process of α-Fe_2O_3 NPs and rGO for an hour.[181] A noteworthy study has been reported, achieving superior electrochemical performance through the unique engineering of nanoarchitecture. A Cu@GNS hybrid material was synthesized *via* facile, inexpensive, and high-yield metal–organic CVD, utilizing Cu(II) acetylacetonate as the metal precursor at 600 °C.[95] The hot-filament CVD (HF-CVD) technique offers an attractive approach to design TMCs (Fe_3C, Co_3C, and Ni_3C) nanocrystalline confined within graphitic shells anchored on vertically aligned GNS nanoribbons.[182] In addition, the arc-discharge offers an appealing route for preparing Ni-coated GNS hybrids *via* the use of a direct current (DC) arc discharge generated in a He/CH_4 environment at a pressure of 0.08 MPa and a current of 40 A. Cong and coauthors reported the deposition of NGNS/C-encapsulated Si NPs onto carbon nanofibers (CNFs) through surface alteration, electrostatic self-assembly, cross-linking with thermal treatment, and carbonization (Fig. 11b).[180]

Initially, CNF was prepared by a co-precipitation method, and Si–NH_2 was achieved by modifying the surface of Si NPs with APTES. After that, the N-GNS/C@Si/CNF hybrid was produced by mixing Si–NH_2, CNF, and GO through a simple physical process to form a highly stable dispersion. Then, formaldehyde and melamine were added under stirring conditions, followed by transferring the solution into a Teflon-lined stainless-steel autoclave for a hydrothermal reaction at 180 °C for 12 hours. The product obtained after hydrothermal synthesis was dried and then heated to 800 °C in Ar gas for 5 hours to obtain the final product. Table 2 summarizes the advantages and disadvantages of different synthesis methods for fabricating the active metallic nanostructures-encapsulated carbon hybrid materials towards electrocatalysis applications.

ORR, HER, and OER applications of core–shell hybrid catalysts

ORR applications

Electrochemical fuel cell devices generate electricity directly from the chemical reactions of fuels. In the reaction mechanism, ORR at the cathode end is relatively sluggish compared to

Table 2 Common synthesis method for core–shell catalysts and their key advantages and limitations

Synthesis methods	Advantages	Disadvantages
Hydrothermal/solvothermal method	- Facile to manage reaction stoichiometry, ease, cost-effectiveness, and precise control of the morphology/size distribution/composition	- Safety issues due to organic solvent usage, and difficulty in directly seeing the reaction progress
Ultra-sonication method	- Facile method with rapid reaction rates and short time, accurately control composition/structure, facile processing, and potential for large-scale production, cost effectiveness	- This method requires high equipment costs, and it is restricted to adhesion between the substrate and the catalyst
Co-assembly method	- Facile and scalable method, the material can be formed with high purity, composition, and the type of catalyst can be easily controlled	- Complex optimization process, difficult to achieve uniform shell thickness, challenge of template removal without destroying the catalyst structure
Thermal treatment method	- Generation of finely controlled catalyst NPS covered by carbon shell, potential for high-density TM@C formation	- High temperature, requirement of specialized equipment, challenge for large-scale production, and critical control of synthesis process parameters

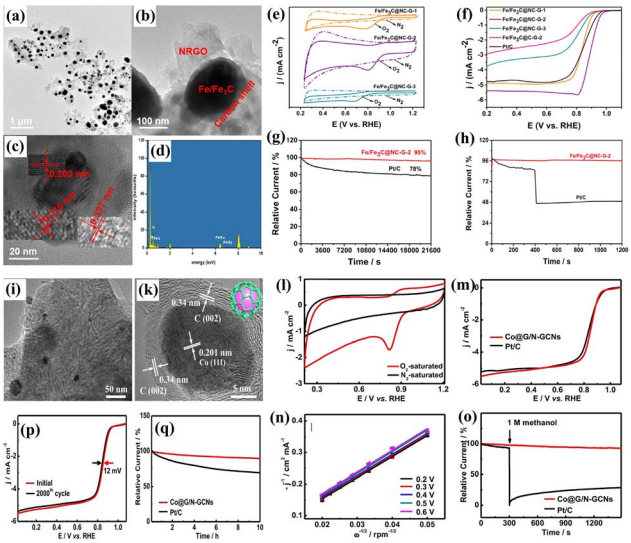

Fig. 12 (a) TEM, (b) HR-TEM, (c-d) EDS analysis, and (e) BET measurement of the FeP NPs embedded in N,P–C layers (reproduced from ref. 153 with permission from Elsevier, copyright 2019); TEM images of (f–h) FeP/N-GNS and (i–k) NiP/N-GNS, and (l–o) their XPS analysis (reproduced from ref. 157 with permission from Cell Press, copyright 2019).

hydrogen oxidation at the anode. Thus, most of the study is to overcome the slow reaction rate of ORR in order to deliver high device efficiency. The carbon layer in a core–shell structure with metals offers various benefits, including improved catalytic activity, stability, and lifetime of the nanomaterial, due to its ability to disperse metal nanoparticles uniformly and prevent their undesirable dissolution and agglomeration. Zhang and coauthors reported synthesizing Fe/Fe_3C@NC-GNS hybrid (Fig. 12a–d),[183] which presents an outstanding ORR performance in terms of a high onset potential (E_{onset}) of 0.97 V and half-wave potential ($E_{1/2}$) of 0.88 V, respectively, reaching those of the commercial Pt/C in alkaline solution (Fig. 12e and f). In addition, the Fe/Fe_3C@NC-GNS exhibits stable operation with a 95% retention rate, indicating outstanding running stability (Fig. 12g). The excellent resistance to the methanol crossover effect further demonstrates its high applicability as an ORR electrocatalyst (Fig. 12h). Liang and coauthors recently demonstrated this effect using a hybrid of Co_3O_4 encapsulated within rGO towards ORR.[33] While Co_3O_4 and rGO individually exhibit insufficient activity, the formation of core–shell hybrid demonstrated remarkable ORR performance, delivering comparable catalytic behaviour to Pt in alkaline media but with superior stability.

In another study, Jin and co-authors developed a g-C_3N_4@-cobalt oxide core–shell hybrid supported by GNS-derived catalyst, which exhibited high activity and stability as an ORR electrocatalyst.[184] They demonstrated that the developed catalyst exhibited outstanding ORR performance with a predominant 4e reaction pathway in alkaline. Moreover, its kinetic-limiting current density was nearly identical to that of commercial Pt/C. The catalytic behavior of the catalyst could be further improved by designing 3D aerogel based on Fe_3O_4 NPs encapsulated within N-GNS. The 3D network of Fe_3O_4 NPs, uniformly decorated on GNS, exhibits enhanced ORR performance in basic media, along with improved J, reduced H_2O_2 generation, a positive onset potential (V_{onset}), and higher electron transfer compared to either Fe_3O_4 NPs/N-carbon black or individual NGNS, alongside durability that outperforms Pt/C.[185] The development of TMOs encapsulated GNS-based hybrid nanostructures has garnered significant attention due to their unique structure and physicochemical properties. Lin and coauthors designed a petal-like $NiCo_2O_4$ covered with rGO nanosheets hybrid structure (2D $NiCo_2O_4$ nanoflowers/rGO). This good coupling offers more positive onset potential (0.92 V), high charge transfer, good durability of 10 000 s continuous operation with 93.6% retention.[177] Recently, a core–shell composite of FeCo@NC within GNS was designed, exhibiting a desirable electrode potential of 0.87 V and superior durability.[96] Furthermore, N-doped carbon layers with covalently anchored $Co_{0.5}Fe_{0.5}S$ have the potential to improve ORR performance. Specifically, the covalent attachment between the carbon layer and active sulfide nanoparticles, along with the dispersion and precise addition of Fe in the sulfide structure, can accelerate electron/mass transport with adequate O_2 adsorption and activation, thereby providing a high half-wave potential of 0.808 V and long-term stability.[120] In another report,[129] a Co_3ZnC/Co nanojunction anchored on N-GNS layers was fabricated for use as an ORR electrocatalyst, indicating the efficiency of TMCs. The catalyst demonstrated superior performance with an onset potential of 0.912 V. Similarly, Fan and coauthors reported outstanding ORR activity of M_3C (M = Fe, Co, Ni) nanocrystals encapsulated within GNS nanoribbons with a low Tafel slope, high onset potential, high transfer number approximately 4, and remarkable durability with no performance decay during 20 000 s.[182] Similarly, other studies have reported superior ORR performance with an N-GNS layer doped with Fe atoms and coated with Fe_3C NPs.[132] A representative study has been reported that substantiates and reinforces the effectiveness of this technique. Jiang and coauthors found that a specific nanostructure could achieve comparably superior catalytic activity than Pt/C when annealed at 800 °C, with its behavior deviating from ideal performance at annealing temperatures either lower than 700 °C or higher than 900 °C. TMNs, such as homogeneously distributed FeN NPs anchored on microporous GNS aerogel, have also been studied to investigate their ORR performance.[143,186] The improved performance could be attributed to the large specific surface area, porosity, high density of Fe atoms, smaller Fe_xN NPs size, and the synergistic effect brought about by the strong contact between NPs and GNS. Notably, it delivered activity on par with Pt while demonstrating superior stability and alcohol tolerance. Recently, Amiinu and co-authors designed a core–shell nanostructure by combining TMNs/TMSs and graphitic carbon to achieve a favorable electrochemical performance.[187] This material features excellent flexibility, a large surface area, and an interconnected porous network with a hierarchical architecture, thereby offering various advantages, including a high onset potential of 0.9 V and a charge transfer number of approximately 3.96. There are also numerous reports that have

Table 3 The ORR, HER, and OER performance of different core–shell nanostructure electrocatalysts

Material	HER (mV)	OER (mV)	ORR ($E_{1/2}$) V	Electrolyte	References
CoFe@NC/NCHNSs	120	285	0.92	0.1 M KOH (ORR), 1.0 M KOH (HER/OER)	197
CoP/C NWs	40.1	230	0.85	0.1 M KOH (ORR), 1.0 M KOH (HER/OER)	198
FeS/Fe_3C@Fe–N–C	—	276	0.91	0.1 M KOH (ORR), 1.0 M KOH (OER)	199
NC@Fe_3C-900	—	—	0.98	0.1 M KOH	200
CoSnOH/S@C NPs		137	0.88	0.1 M KOH (ORR), 1.0 M KOH (OER)	201
FeNiPt@C NFs	25	294	0.93	0.1 M KOH (ORR), 1.0 M KOH (HER/OER)	202
CS-NFO@PNC-700	200	217	0.85	0.1 M KOH (ORR), 1.0 M KOH (HER/OER)	203
IrCo@NCNT/PC	37	240	0.83	0.1 M KOH (ORR), 1.0 M KOH (HER/OER)	204
CoFeN-NCNTs//CCM	151	320	0.84	0.1 M KOH (ORR), 1.0 M KOH (HER/OER)	205
Co_{NPs}/NC/CeO_2	—	230	0.86	0.1 M KOH	206
Ni_1Co_3/N-CNTs-2	—	400	0.85	0.1 M KOH	207
RuNi/Ni@C–CNF	9	—	—	1 M KOH	208
Ni_3Fe@NCS	212.2	288.8	—	1.0 M KOH	209
Ce–NiCoP@C/NF	37	255	—	1.0 M KOH	210
Co@CNS_{100}	—	301	—	1.0 M KOH	211
HEAs@ACWs	7	—	—	1.0 M KOH	212
LDH/CNT/CC	—	200	—	1.0 M KOH	213
Co/Co_9S_8@NSC-2	—	139	0.88	0.1 M KOH	214
$PtNi_{SA-NPs}$/NDCF	24.7	—	0.91	0.1 M $HClO_4$ (ORR) and 0.5 M H_2SO_4 (HER)	215
Co_2P@NPC/CPE	173	349	—	1.0 M KOH	216
NT@NC-8	326	355	0.64	0.1 M KOH (ORR), 1.0 M KOH (HER/OER)	217
FeNiP/NC	—	240	—	1.0 M KOH	218
FeCoP@NC	—	—	0.86	1.0 M KOH	219
Fe–Co_2P/CoP@CNT NCPs	138	296.7	—	1.0 M KOH	220
Fe–Co_2P@Fe–N–C	77	300	0.88	0.1 M KOH	221
Ni_xCo_{1-x}@Ni_xCo_{1-x}O/NCNT	74	380	0.79	0.1 M KOH (ORR), 1.0 M KOH (HER/OER)	222
Co/N–CNF	241	380	0.86	0.1 M KOH (ORR/OER), 1.0 M KOH (HER)	223
Co@IC/MoC@PC	68	277	0.875	0.1 M KOH (ORR), 1.0 M KOH (HER/OER)	224
Ni–Pd–P/C	—	330	0.923	0.1 M KOH (ORR), 1.0 M NaOH (OER)	225
Ni@Ni-NC	—	371	—	1.0 M KOH	226
Fe, Co/N–C	249	388	0.86	1.0 M KOH	227
CoP_2/Co_2P@CNT-CC	94.4	280	—	1.0 M KOH	228
Co_2P/Co@N-CNT/NPG	86	309	0.91	0.1 M KOH (ORR), 1.0 M KOH (HER/OER)	229
CoNiP/CoNi/N−RGO	160	300	—	1.0 M KOH	230
Ir@N-G-600	92.5	314		1.0 M KOH (HER), 0.5 M H_2SO_4 (OER)	231
Ni_3FeN/VN–NG	—	230	0.87	0.1 M KOH	232
$CoFe_2O_4$/rGO	343	421	—	1.0 M KOH	233
3D Fe–N/P-G	—	420	0.86	0.1 M KOH	234
NS/G-AD	—	350	0.87	0.1 M KOH	235
FeNi/$(FeNi)_9S_8$/N,S–CNS	—	283	0.86	0.1 M KOH (ORR), 1.0 M KOH (OER)	236
Co@NC/rGO	—	—	0.86	0.1 M KOH	237
NiFe–N-CNT–rGO	—	270	—	1.0 M KOH	238
FeCoMoS@NG	137	238	0.83	0.1 M KOH (ORR), 1.0 M KOH (HER/OER)	239
Ni_2P@NSG	110	240	—	1.0 M KOH	240
Re–Ni_3S_2/NG/NF	100	247	0.66	1.0 M KOH	241

demonstrated the application of core–shell nanoarchitecture derived from carbon structures to enhance ORR catalytic activity.[188–190]

Niu and coauthors developed GNS-encapsulated Co NPs embedded in porous N–C NSs (Fig. 12i–k),[191] which show exceptional ORR activity with a half-wave potential of 0.86 V and electron transfer number (n) values of 3.96, similar to 3.94 of Pt/C (Fig. 12l–n). The alcohol crossover effect and stability tests of the catalysts demonstrate high methanol resistance, with only ~a 12 mV decay of the half-wave potential after 2000 cycles, significantly better than that of Pt/C (20 mV) (Fig. 12o–p). In addition, the amperometry test for ORR indicates that the developed catalyst maintains 89% of its initial current density value, which is superior to that of Pt/C (69%) (Fig. 12q), demonstrating the intensely improved durability of the catalyst. Various core–shell electrocatalysts have been developed for ORR applications, and their performance is compared in Table 3.

HER applications

Water electrolysis is a promising technology for generating green hydrogen, offering a carbon-neutral alternative to hydrogen derived from fossil fuels. In this process, electric current is utilized to split water into H_2 and O_2, thus making this technology a potential solution of clean and renewable energy for the future. Despite its potential, water electrolysis

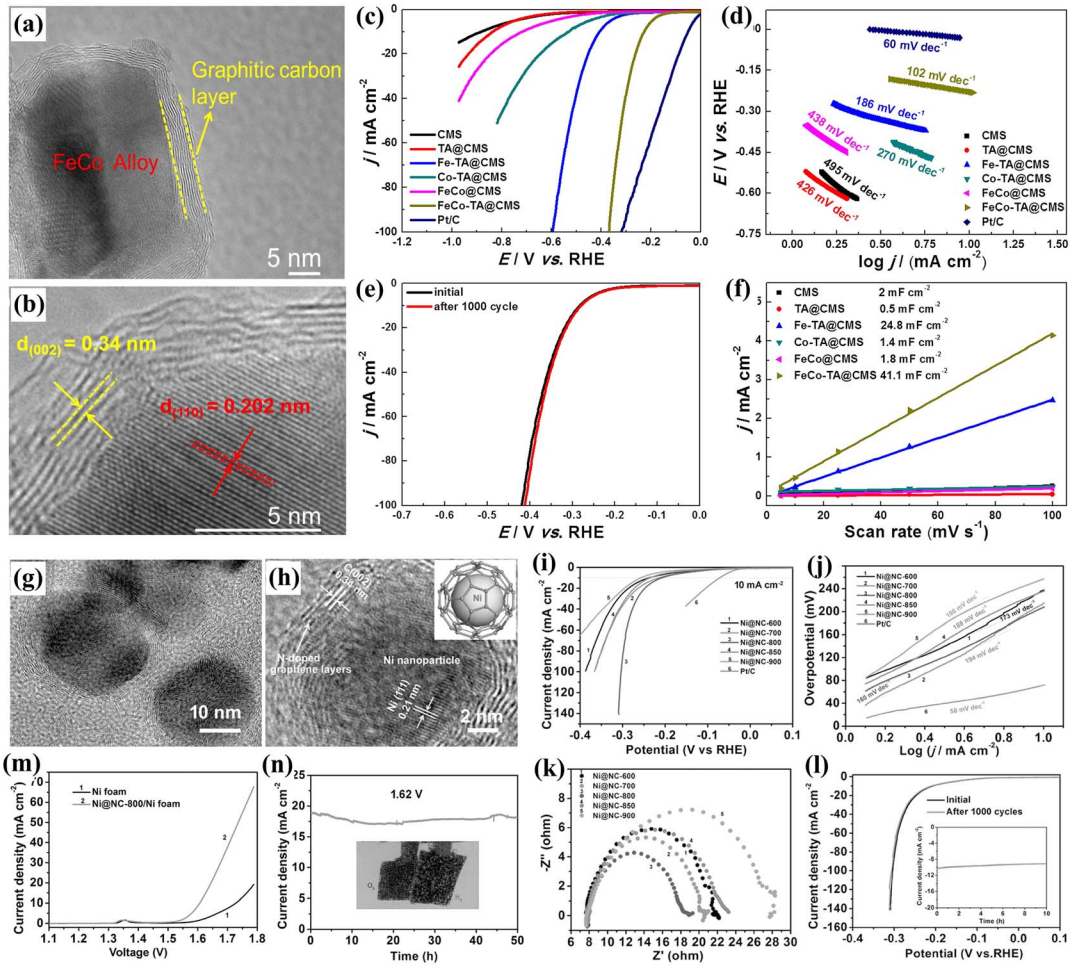

Fig. 13 (a and b) TEM images and (c–f) HER properties of N-doped graphitic carbon shell-encapsulated FeCo alloy material (reproduced from ref. 192 with permission from Elsevier, copyright 2021); (g and h) TEM images and (i–l) HER properties of Ni NPs encapsulated in few-layer N-GNS material, (m and n) water splitting process based on Ni NPs encapsulated in few-layer N-GNS material[195] (reproduced from ref. 195 with permission from Wiley, copyright 2016).

doesn't achieve theoretical efficiency because the sluggish OER kinetics require a high overpotential, resulting in energy losses. Specifically, hydrogen is crucial for decarbonizing hard-to-abate sectors, such as the steel industry. Therefore, designing suitable electrocatalysts to perform the hydrogen evolution reaction at a lower overpotential has been a hot topic for over a decade. Based on experimental results and theoretical modeling, core–shell nanostructure design prevents the accumulation, leaching, and corrosion of the hybrid catalyst in electrolyte media, thereby creating a large number of electroactive sites. In this manner, the catalyst could achieve superior catalytic activity as well as stability. Liu and coauthor introduced a hybrid of FeCo alloy NPs with a diameter around 50 nm embedded in a porous *N*–C layers (Fig. 13a and b), which needs an overpotential of 233 mV at 10 mA cm^{-2} for fast kinetics of HER along with the excellent stability after a continuous CV scanning for 1000 cycles in 1 M KOH (Fig. 13c–e).[192] The high ECSA is favorable for exposing electrochemically accessible active sites, thereby facilitating the interaction between active sites and the electrolyte solution, which leads to high catalytic efficiency (Fig. 13f). Recently, highly dispersed Co NPs confined by Co,N–C have been introduced as efficient HER electrocatalysts, exhibiting a low overpotential of 10 mA cm^{-2}, which significantly outperforms previous non-precious metal catalysts.[193] Zeng and coauthors reported the development of N-enriched multilayer GNS shells decorated with metallic Co NPs, which indicates the crucial catalytic active centers of Co–N–C moieties for HER in alkaline media. The catalyst delivered an overpotential of 220/183 mV at J value of 10 mA cm^{-2} and Tafel slope of 112/100 mV dec^{-1} in alkaline/acidic medium.[171] The TMCs, for example, Mo_2C coupled with rGO, were developed for efficient HER, offering an overpotential of ~34 mV to reach 10 mA cm^{-2}, surpassing that of commercial Pt/C (40 mV).[194] Moreover, the as-developed catalyst has a 33.6 mV dec^{-1} Tafel slope, which is quite comparable to that of Pt/C (30 mV dec^{-1}), indicating the synthesis of an exceptional nanomaterial for high-efficiency HER performance. The theoretical and experimental findings elucidate the synergy between Mo_2C and C-pyridinic N, which facilitates rapid adsorption/desorption of hydrogen for the HER process, with $\Delta G_{H^*} = -0.22$ eV. Lately, TMPs-based electrocatalysts have demonstrated competitive HER and OER activity, compared to other compounds. Conceptually, introducing

phosphorous atoms into TM crystal lattices enhances the HER performance because phosphorus's high electronegativity draws electrons from TM atoms and creates positively charged H^+ ions that bond with phosphorous atoms, thus acting as Lewis bases. Pu and coauthors reported that FeP nanoparticles encapsulated within N,P–C layer exhibit excellent activity across the entire pH range for HER.[152] The catalyst can deliver overpotentials of 130 mV in an acidic medium, reaching a current density of 10 mA cm^{-2}. Furthermore, the catalytic performance remained nearly unchanged after 10 h of continuous operation in all pH conditions, confirming that the carbon encapsulation effectively protects FeP NPs from corrosion. In another noteworthy study, Wang and coauthors achieved a significant HER performance, including low overpotential (89 mV at 10 mA cm^{-2}), and Tafel slope (76 mV dec^{-1}).[170] This catalytic activity is attributed to the synthesis of an N,P–C layer shell-encapsulated Cu3P NPs, which offer various advantages, including a large specific surface area with a hierarchical porous architecture, as well as a layered carbon shell that provides protection for the NPs against the harsh electrolyte environment. Considering another dimension, the reactivity of TMPs towards HER could be further improved by developing a nano-hybrid with GNS sheets.

Li and coauthors reported an architecture composed of tiny MoP NPs coated with rGO sheets, representing one of the most efficient MoP-derived materials for HER in acidic conditions.[196] The developed material exhibited a low overpotential of 218 mV at 10 mA cm^{-2} and a Tafel slope of 57 mV dec^{-1}, attributed to its abundant active centers. Moreover, the structural design endowed the catalyst with excellent durability, maintaining nearly identical performance even after 1000 cycles.

Xu and coauthor developed Ni NPs encapsulated in few-layer N-GNS *via* a Ni-based MOF-based precursor.[195] The resulting Ni@N-GNS material, featuring numerous sphere-like nanostructures with diameters of 20–30 nm, exhibits highly efficient and stable electrocatalytic activity for HER by obtaining a current density of 10 mA cm^{-2} at an overpotential of 70 mV (Fig. 13g–l). The overall water splitting process based on the developed material achieves a current density of 10 mA cm^{-2} at a cell voltage of 1.60 V and remains stable for at least 50 hours (Fig. 13m–n), comparable to many reported electrocatalysts. A recent report by Zhang and co-authors proposed a novel nanostructure based on TMPs (MoP) and TMCs (MoC) decorated with carbon layers. Such architecture was able to achieve remarkable performance over a wider pH range compared to MoP, Mo_2C, and their mixture.[158] The nanomaterials delivered lower V_{over} of 89, 136, and 75 in acid (pH = 0), neutral (pH = 7), as well as base (pH = 14) media, alongside long-term durability. So far, many studies have focused on developing core–shell electrocatalysts to improve HER performance, as shown in Table 3.

OER applications

In reference to OER, Feng and co-authors fabricated N-GNS decorated with NiFe NPs,[242] resulting in the superior OER reaction kinetics, attributed from its small particle size (~16 nm), that leads to ample number of active sites alongside large specific surface area (2.98 mF cm^{-2}), which is smaller than other comparative samples with particle size ~61/33 nm and reported surface area of 2.25/2.61 mF cm^{-2}. The optimized material exhibited an impressively low overpotential of 281 mV at a current density of 10 mA cm^{-2} and a Tafel slope of 53 mV dec^{-1}, both of which are smaller than those from IrO_2/C and previous Ni-derived materials. Fe and Co-based bimetallic alloy encapsulated within N–C anchored within N-GNS[96] delivered an exceptional electrochemical performance with an overpotential of 440 mV at 10 mA cm^{-2} and a small Tafel slope (90 mV dec^{-1}), owing to their synergistic effect arising from FeCo NPs as well as N–C layer. Interestingly, another noteworthy report by Shen and coauthors investigated the transformation of iron-cobalt into iron-cobalt sulfide NPs through encapsulation *via* covalent interaction with a mesoporous N–C layer.[120] The developed material can achieve an overpotential of 410 mV at 10 mA cm^{-2} and a Tafel slope of 159 mV dec^{-1}. Cui and coauthors directly synthesize monolayer GNS encapsulating uniform TMs NPs, such as Fe, Co, Ni, and their alloys, which immensely boosts the charge transfer from the core metals to the GNS surface (Fig. 14a and b), thereby efficiently optimizing the electronic properties for improving OER activity (Fig. 14c and d).[243] They found that the FeNi alloy encapsulated in GNS exhibits the highest OER activity in alkaline with an overpotential of only 280 mV at 10 mA cm^{-2} while maintaining high durability during 10 000 cycles, superior to commercial IrO_2 (Fig. 14e–h). Su and coauthors successfully proposed the use of TMCs confined within N-GNS for the OER.[129] The unique Co_3ZnC/Co nanojunction architecture confined in N-GNS layers exhibited an overpotential as low as 366 mV at 10 mA cm^{-2}, along with a Tafel slope of 81 mV dec^{-1} and excellent durability after 5000 cycles. This performance surpasses that of Pt/C and RuO_2 in alkaline medium. Recently, Zhang and co-authors designed an intriguing nanoarchitecture featuring a uniform dispersion of hollow Ni_5P_4/Fe_3P nanocubes coated with NC sheets.[245] The distinctive construction and composition of this material enable remarkable electrocatalytic activity with an overpotential of 252 mV to reach 10 mA cm^{-2} and deliver exceptional kinetics, evidenced by a low Tafel slope (24.0 mV dec^{-1}). Interestingly, the catalyst exhibited outstanding electrocatalytic and mechanical durability, even working at a high current of 250 mA cm^{-2}, further suggesting that the material holds great potential as a replacement for commercial Pt-based OER electrocatalysts. Cui and coauthors studied theoretical modeling to decipher the benefits of anchoring the FeNi NPs on carbon layers for a high-performance OER process.[246] Asbemarz and coauthors present a novel bimetallic Fe–Ni MOF anchored on rGO (Fig. 14i and j).[244] The stronger Fe–O bond promotes effective proton and charge transfer, facilitating the OER rate (Fig. 14k). The developed material exhibits high OER performance with a required overpotential of 217 mV at 10 mA cm^{-2}, while maintaining stable catalytic activity with a 16.1% decrease in current density over 100 h (Fig. 14l–q). The improvement in OER activity through the development of core–shell electrocatalysts is also reported in many other studies in Table 3.

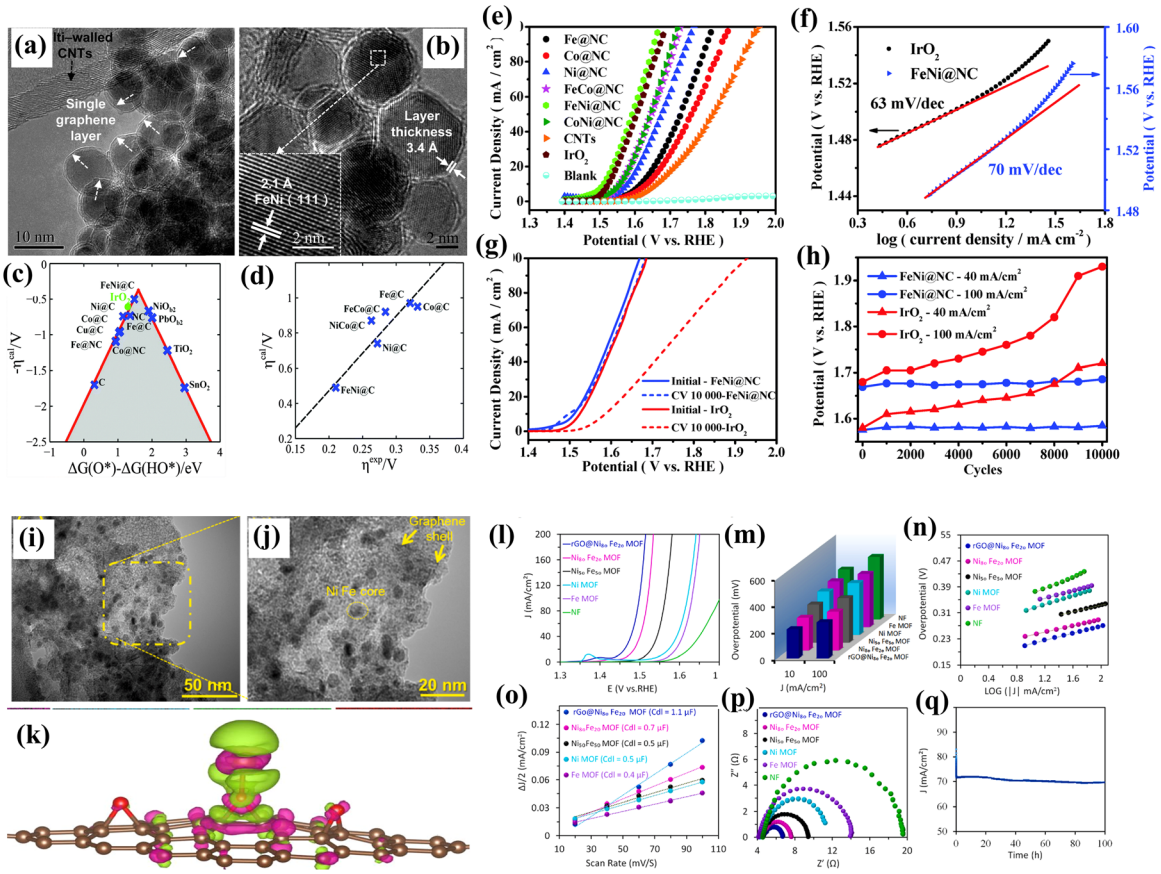

Fig. 14 (a and b) TEM images of the FeNi alloy-confined GNS layer, (c and d) The calculated properties of different materials for OER, (e and h) electrochemical performance of FeNi alloy-confined GNS layer for OER (reproduced from ref. 243 with permission from RSC, copyright 2016); (i and j) TEM images of iron-nickel MOF anchored on rGO, (k) electronic state of Fe–O bond in the hybrid, (l and q) OER performance of the iron-nickel MOF anchored on rGO (reproduced from ref. 244 with permission from Elsevier, copyright 2025).

Challenges, potential solutions, and future research directions

Research on potential materials with high catalytic activity and durability is crucial for a range of electrochemical energy storage and conversion applications, including fuel cells, batteries, and water electrolysis. In this context, constructing unique nanostructures confined within carbon support has emerged as a promising strategy. Such a nano-hybrid offers various advantages, including ample electrocatalytic active sites, electrical conductivity, and a high specific surface area, thereby serving as an ideal alternative to precious-metal-based catalysts, with comparatively high cost-effectiveness, eco-friendliness, and appreciable performance. We have provided a scientific overview of recent advancements in the preparation of core–shell materials. Despite the potential of the metallic nanostructures-encapsulated carbon hybrid materials, significant research challenges remain for their fundamental catalytic mechanisms, synthesis, and long-term stability. Specifically, the catalytic center remains unclear, and the complex dynamics of charge transfer at the interface between the metal core and the carbon shell remain poorly understood. In addition, obtaining good control over the number of carbon layers and defects during synthesis is difficult to optimize fast charge transfer while maximizing the anticorrosion effect. Among the various synthesis routes, hydrothermal/solvothermal methods and electrostatic self-assembly have attracted considerable attention due to their simplicity, cost-effectiveness, and suitability for large-scale production. However, these approaches often suffer from limited product quality and poor controllability over structural and compositional features. In another regard, thermal treatment *via* CVD has demonstrated high synthetic efficiency, combined with ease of large-scale production; however, this process is relatively expensive. In future research directions, *operando* and *in situ* analysis techniques should be applied to clarify structural evolution and find the main active sites during catalytic reactions. Development of new industrial-scale synthesis strategies for fabricating scalable metal-encapsulated carbon hybrids. In this context, combining the experimental approach with theoretical study, such as DFT, machine learning, and AI, will be an effective approach to produce core–shell catalyst materials, which can offer a precise control of their structure, a good understanding of their catalytic mechanism, and a scalable and precise synthesis method with low production cost and high yield. The precise synthesis

of high-quality, controllable materials is expected to elevate catalytic performance and stability, offering extensive potential of metallic nanostructures-encapsulated carbon hybrid in electrochemical applications.

Author contributions

Nguyen Chi Thanh: Conceptualization, Investigation, Methodology, Visualization, Writing-original draft, Writing-review& editing.

Conflicts of interest

There are no conflicts to declare.

Data availability

No primary research results have been included and analysed as part of this review.

Acknowledgements

The author would like to thank Ho Chi Minh City University of Technology and Engineering, Vietnam for financial support.

References

1 A. A. Gewirth and M. S. Thorum, *Inorg. Chem.*, 2010, **49**, 3557–3566.
2 J. Tollefson, *Nature*, 2010, **464**, 1262–1264.
3 C. Sealy, *Mater. Today*, 2008, **11**, 65–68.
4 A. A. Gewirth, J. A. Varnell and A. M. DiAscro, *Chem. Rev.*, 2018, **118**, 2313–2339.
5 H. Lee, M. J. Kim, T. Lim, Y.-E. Sung, H.-J. Kim, H.-N. Lee, O. J. Kwon and Y.-H. Cho, *Sci. Rep.*, 2017, **7**, 5396.
6 C. Lyu, J. Yang, H. Guo, J. Cheng, D. Geng and Y. Liu, *Coord. Chem. Rev.*, 2026, **551**, 217393.
7 C. Lyu, C. Cao, J. Cheng, Y. Yang, K. Wu, J. Wu, W. M. Lau, P. Qian, N. Wang and J. Zheng, *Chem. Eng. J.*, 2023, **464**, 142538.
8 J. Cheng, C. Lyu, H. Li, J. Wu, Y. Hu, B. Han, K. Wu, M. Hojamberdiev and D. Geng, *Appl. Catal., B*, 2023, **327**, 122470.
9 Y. Tokura and N. Nagaosa, *Science*, 2000, **288**, 462–468.
10 R. R. Chianelli, G. Berhault and B. Torres, *Catal. Today*, 2009, **147**, 275–286.
11 S. T. Oyama, *J. Catal.*, 2003, **216**, 343–352.
12 S. T. Oyama, *Catal. Today*, 1992, **15**, 179–200.
13 Z. Chen, D. Higgins, A. Yu, L. Zhang and J. Zhang, *Energy Environ. Sci.*, 2011, **4**, 3167.
14 H. Zhao, J. T. Ren and Z. Y. Yuan, *Coord. Chem. Rev.*, 2024, **514**, 215901.
15 W. Chen, Y. Qin, C. Heng, S. Wang, M. Ge, Y. Li, X. Wan, X. Li, J. Shui, Y. Su and D. Su, *J. Am. Chem. Soc.*, 2025, **147**, 35730–35741.
16 H. Zhao and Z.-Y. Yuan, *Smart Mater. Devices.*, 2025, **1**, 202521.
17 S. D. Perera, R. G. Mariano, K. Vu, N. Nour, O. Seitz, Y. Chabal and K. J. Balkus, *ACS Catal.*, 2012, **2**, 949–956.
18 B. Kirubasankar, V. Murugadoss and S. Angaiah, *RSC Adv.*, 2017, **7**, 5853–5862.
19 S. Wu, Z. Yin, Q. He, G. Lu, Q. Yan and H. Zhang, *J. Phys. Chem. C*, 2011, **115**, 15973–15979.
20 S. Wu, Z. Yin, Q. He, X. Huang, X. Zhou and H. Zhang, *J. Phys. Chem. C*, 2010, **114**, 11816–11821.
21 X. W. Liu, J. J. Mao, P. De Liu and X. W. Wei, *Carbon*, 2011, **49**, 477–483.
22 Q. H. Hu, X. T. Wang, H. Chen and Z. F. Wang, *New Carbon Mater.*, 2012, **27**, 35–41.
23 R. Jiang, X. Zhou and Z. Liu, *Mater. Sci. Eng., A*, 2017, **679**, 323–328.
24 T. Duy Thanh, N. Dinh Chuong, H. Van Hien, T. Kshetri, L. Huu Tuan, N. Hoon Kim and J. Hee Lee, *Prog. Mater. Sci.*, 2018, **96**, 51–85.
25 J. Wang, F. Ma, W. Liang and M. Sun, *Mater. Today Phys.*, 2017, **2**, 6–34.
26 W. Choi, N. Choudhary, G. H. Han, J. Park, D. Akinwande and Y. H. Lee, *Mater. Today*, 2017, **20**, 116–130.
27 Z. Jin, D. Nackashi, W. Lu, C. Kittrell and J. M. Tour, *Chem. Mater.*, 2010, **22**, 5695–5699.
28 J. H. Jang, A. A. Jeffery, J. Min, N. Jung and S. J. Yoo, *Nanoscale*, 2021, **13**, 15116–15141.
29 J. Zhao, M. Kou, Q. Yuan, Y. Yuan and J. Zhao, *Molecules*, 2024, **29**, 4677.
30 Z.-S. Wu, S. Yang, Y. Sun, K. Parvez, X. Feng and K. Müllen, *J. Am. Chem. Soc.*, 2012, **134**, 9082–9085.
31 R. Kumar, R. K. Singh, P. K. Dubey, D. P. Singh, R. M. Yadav and R. S. Tiwari, *Adv. Mater. Interfaces*, 2015, **2**, 1–13.
32 W. Qiu, J. Jiao, J. Xia, H. Zhong and L. Chen, *Chem. - Eur. J.*, 2015, **21**, 4359–4367.
33 Y. Liang, Y. Li, H. Wang, J. Zhou, J. Wang, T. Regier and H. Dai, *Nat. Mater.*, 2011, **10**, 780–786.
34 J. Guo, F. Li, Y. Sun, X. Zhang and L. Tang, *Electrochim. Acta*, 2015, **167**, 32–38.
35 X. Xiao, J. R. Michael, T. Beechem, A. McDonald, M. Rodriguez, M. T. Brumbach, T. N. Lambert, C. M. Washburn, J. Wang, S. M. Brozik, D. R. Wheeler, D. B. Burckel and R. Polsky, *J. Mater. Chem.*, 2012, **22**, 23749.
36 X. Cui, Y. Li, S. Bachmann, M. Scalone, A. E. Surkus, K. Junge, C. Topf and M. Beller, *J. Am. Chem. Soc.*, 2015, **137**, 10652–10658.
37 F. Yang, T. Qiu, C. Chi, S. Liang, L. Deng, X. Wang, C. Wang, J. Fu, Y. Wang and Y. Li, *Chem. Eng. J.*, 2017, **330**, 880–889.
38 S. Yang, X. Feng, S. Ivanovici and K. Müllen, *Angew. Chem., Int. Ed.*, 2010, **49**, 8408–8411.
39 R. Mo, D. Rooney, K. Sun and H. Y. Yang, *Nat. Commun.*, 2017, **8**, 1–9.
40 H. Yuan, L. Kong, T. Li and Q. Zhang, *Chin. Chem. Lett.*, 2017, **28**, 2180–2194.
41 J. Liu, E. Li, M. Ruan, P. Song and W. Xu, *Catalysts*, 2015, **5**, 1167–1192.
42 X. Zhou, J. Qiao, L. Yang and J. Zhang, *Adv. Energy Mater.*, 2014, **4**, 1–25.

43 Y. Yan, B. Y. Xia, B. Zhao and X. Wang, *J. Mater. Chem. A*, 2016, **4**, 17587–17603.
44 A. Wang, C. Wang, L. Fu, W. Wong-Ng and Y. Lan, *Nano-Micro Lett.*, 2017, **9**, 47.
45 A. Gupta, T. Sakthivel and S. Seal, *Prog. Mater. Sci.*, 2015, **73**, 44–126.
46 J. Liu, H. Wang and M. Antonietti, *Chem. Soc. Rev.*, 2016, **45**, 2308–2326.
47 A. Hayat, A. G. Al-Sehemi, K. S. El-Nasser, T. A. Taha, A. A. Al-Ghamdi, J. Ali Shah Syed, M. A. Amin, T. Ali, T. Bashir, A. Palamanit, J. Khan and W. I. Nawawi, *Int. J. Hydrogen Energy*, 2022, **47**, 5142–5191.
48 J. Zhu, P. Xiao, H. Li and S. A. C. Carabineiro, *ACS Appl. Mater. Interfaces*, 2014, **6**, 16449–16465.
49 A. Zambon, J.-M. Mouesca, C. Gheorghiu, P. A. Bayle, J. Pécaut, M. Claeys-Bruno, S. Gambarelli and L. Dubois, *Chem. Sci.*, 2016, **7**, 945–950.
50 Y. Zhao, J. Zhang and L. Qu, *ChemNanoMat*, 2015, **1**, 298–318.
51 G. Dong, Y. Zhang, Q. Pan and J. Qiu, *J. Photochem. Photobiol., C*, 2014, **20**, 33–50.
52 Y. Zheng, Y. Jiao, Y. Zhu, L. H. Li, Y. Han, Y. Chen, A. Du, M. Jaroniec and S. Z. Qiao, *Nat. Commun.*, 2014, **5**, 1–8.
53 J. A. A. Hutapea, Y. G. O. Manik, S. T. C. L. Ndruru, J. Huang, R. Goei, A. I. Y. Tok and R. Siburian, *Micro*, 2025, **5**, 40.
54 N. D. Chuong, T. D. Thanh, N. H. Kim and J. H. Lee, *ACS Appl. Mater. Interfaces*, 2018, **10**, 24523–24532.
55 J. Gautam, T. Duy, K. Maiti, N. Hoon and J. Hee, *Carbon*, 2018, **137**, 358–367.
56 T. Duy, N. Dinh, H. Van Hien, T. Kshetri and L. Huu, *Prog. Mater. Sci.*, 2018, **96**, 51–85.
57 H. V. Hien, T. D. Thanh, N. D. Chuong, D. Hui, N. H. Kim and J. H. Lee, *Composites, Part B*, 2018, **143**, 96–104.
58 K. Gopalsamy, J. Balamurugan, T. Duy, N. Hoon, D. Hui and J. Hee, *Composites, Part B*, 2018, **143**, 319–327.
59 P. Solís-Fernández, M. Bissett and H. Ago, *Chem. Soc. Rev.*, 2017, **46**, 4572–4613.
60 H. M. Jeong, J. W. Lee, W. H. Shin, Y. J. Choi, H. J. Shin, J. K. Kang and J. W. Choi, *Nano Lett.*, 2011, **11**, 2472–2477.
61 H. Jin, C. Guo, X. Liu, J. Liu, A. Vasileff, Y. Jiao, Y. Zheng and S.-Z. Qiao, *Chem. Rev.*, 2018, **118**(13), 6337–6408.
62 L. Qu, Y. Liu, J.-B. Baek and L. Dai, *ACS Nano*, 2010, **4**, 1321–1326.
63 K. Gopalsamy, J. Balamurugan, T. D. Thanh, N. H. Kim and J. H. Lee, *Chem. Eng. J.*, 2017, **312**, 180–190.
64 T. D. Thanh, N. D. Chuong, H. Van Hien, N. H. Kim and J. H. Lee, *ACS Appl. Mater. Interfaces*, 2018, **10**, 4672–4681.
65 A. Pani, T. D. Thanh, N. H. Kim, J. H. Lee and S.-I. Yun, *IET Nanobiotechnol.*, 2016, **10**, 431–437.
66 T. D. Thanh, J. Balamurugan, N. T. Tuan, H. Jeong, S. H. Lee, N. H. Kim and J. H. Lee, *Biosens. Bioelectron.*, 2017, **89**, 750–757.
67 T. D. Thanh, J. Balamurugan, H. V. Hien, N. H. Kim and J. H. Lee, *Biosens. Bioelectron.*, 2017, **89**, 750–757.
68 T. D. Thanh, N. D. Chuong, J. Balamurugan, H. Van Hien, N. H. Kim and J. H. Lee, *Small*, 2017, **13**, 1701884.
69 T. Ando, *NPG Asia Mater.*, 2009, **1**, 17–21.
70 Md. S. A. Bhuyan, Md. N. Uddin, Md. M. Islam, F. A. Bipasha and S. S. Hossain, *Int. Nano Lett.*, 2016, **6**, 65–83.
71 H. M. Zhang, J. J. Wang, Y. Meng, F. Lu, M. Ji, C. Zhu, J. Xu and J. Sun, *Energy Mater. Adv.*, 2022, **2022**, 0006.
72 J. Raymond, *J. Electrochem. Soc.*, 1965, **112**, 526.
73 H. Alt, H. Binder and G. Sandstede, *J. Catal.*, 1973, **28**, 8–19.
74 C. W. B. Bezerra, L. Zhang, K. Lee, H. Liu, A. L. B. Marques, E. P. Marques, H. Wang and J. Zhang, *Electrochim. Acta*, 2008, **53**, 4937–4951.
75 D. C. Higgins and Z. Chen, *Can. J. Chem. Eng.*, 2013, **91**, 1881–1895.
76 H. Li, J. Wu, M. Li and Y. Wang, *Catalysts*, 2024, **14**, 368.
77 A. Salamat, A. L. Hector, P. Kroll and P. F. McMillan, *Coord. Chem. Rev.*, 2013, **257**, 2063–2072.
78 Y. Zhong, X. Xia, F. Shi, J. Zhan, J. Tu and H. J. Fan, *Adv. Sci.*, 2016, **3**, 1500286.
79 S. Dong, X. Chen, X. Zhang and G. Cui, *Coord. Chem. Rev.*, 2013, **257**, 1946–1956.
80 Q. Yang, Z. Lu, J. Liu, X. Lei, Z. Chang, L. Luo and X. Sun, *Prog. Nat. Sci.:Mater. Int.*, 2013, **23**, 351–366.
81 F. N. Sayed and V. Polshettiwar, *Sci. Rep.*, 2015, **5**, 1–14.
82 X. Tao, Y. Zhou, Q. Wei, G. Yu, Q. Cui, J. Liu and T. Liu, *Fuel Process. Technol.*, 2014, **118**, 200–207.
83 Z. Li, X. Guo, F. Tao and R. Zhou, *RSC Adv.*, 2018, **8**, 25283–25291.
84 M. G. Taylor, N. Austin, C. E. Gounaris and G. Mpourmpakis, *ACS Catal.*, 2015, **5**, 6296–6301.
85 B. Zhao, X. Ke, J. Bao, C. Wang, L. Dong, Y. Chen and H. Chen, *J. Phys. Chem. C*, 2009, **113**, 14440–14447.
86 J. Li, G. Liu, X. Long, G. Gao, J. Wu and F. Li, *J. Catal.*, 2017, **355**, 53–62.
87 L. Liu, P. Concepción and A. Corma, *J. Catal.*, 2016, **340**, 1–9.
88 W. Zhong, H. Liu, C. Bai, S. Liao and Y. Li, *ACS Catal.*, 2015, **5**, 1850–1856.
89 T. Fu, M. Wang, W. Cai, Y. Cui, F. Gao, L. Peng, W. Chen and W. Ding, *ACS Catal.*, 2014, **4**, 2536–2543.
90 C. Wang, P. Zhai, Z. Zhang, Y. Zhou, J. Zhang, H. Zhang, Z. Shi, R. P. S. Han, F. Huang and D. Ma, *J. Catal.*, 2016, **334**, 42–51.
91 L. Ai, T. Tian and J. Jiang, *ACS Sustain. Chem. Eng.*, 2017, **5**, 4771–4777.
92 X. Li, Z. Niu, J. Jiang and L. Ai, *J. Mater. Chem. A*, 2016, **4**, 3204–3209.
93 W. Zhou, J. Zhou, Y. Zhou, J. Lu, K. Zhou, L. Yang, Z. Tang, L. Li and S. Chen, *Chem. Mater.*, 2015, **27**, 2026–2032.
94 Q. Zhang, Q. Luo, Z. Qin, L. Liu, Z. Wu, B. Shen and W. Hu, *ACS Omega*, 2018, **3**, 3420–3428.
95 S. Wang, X. Huang, Y. He, H. Huang, Y. Wu, L. Hou, X. Liu, T. Yang, J. Zou and B. Huang, *Carbon*, 2012, **50**, 2119–2125.
96 N. Wu, Y. Lei, Q. Wang, B. Wang, C. Han and Y. Wang, *Nano Res.*, 2017, **10**, 2332–2343.
97 Y. Tu, P. Ren, D. Deng and X. Bao, *Nano Energy*, 2018, **52**, 494–500.
98 Y. Feng, X. Y. Yu and U. Paik, *Sci. Rep.*, 2016, **6**, 1–8.

99 Y. Sun, Q. Liu, S. Gao, H. Cheng, F. Lei, Z. Sun, Y. Jiang, H. Su, S. Wei and Y. Xie, *Nat. Commun.*, 2013, **4**, 1–8.
100 L. Xu, Q. Jiang, Z. Xiao, X. Li, J. Huo, S. Wang and L. Dai, *Angew. Chem., Int. Ed.*, 2016, **55**, 5277–5281.
101 Q. Zhang, H. Chen, X. Han, J. Cai, Y. Yang, M. Liu and K. Zhang, *ChemSusChem*, 2016, **9**, 186–196.
102 J. Jin, X. Fu, Q. Liu and J. Zhang, *J. Mater. Chem. A*, 2013, **1**, 10538.
103 K. Maiti, N. H. Kim and J. H. Lee, *Chem. Eng. J.*, 2021, **410**, 128358.
104 H. Quan, B. Cheng, Y. Xiao and S. Lei, *Chem. Eng. J.*, 2016, **286**, 165–173.
105 W. Yaseen, N. Ullah, M. Xie, B. A. Yusuf, Y. Xu, C. Tong and J. Xie, *Surf. Interfaces*, 2021, **26**, 101361.
106 X. Yuan, C. Yin, Y. Zhang, Z. Chen, Y. Xu and J. Wang, *Sci. Rep.*, 2019, **9**, 5807.
107 M. Ishaq, M. Jabeen, W. Song, L. Xu and Q. Deng, *J. Electroanal. Chem.*, 2017, **804**, 220–231.
108 H. Chen, Y. Ai, F. Liu, X. Chang, Y. Xue, Q. Huang, C. Wang, H. Lin and S. Han, *Electrochim. Acta*, 2016, **213**, 55–65.
109 R. Subbaraman, D. Tripkovic, K. C. Chang, D. Strmcnik, A. P. Paulikas, P. Hirunsit, M. Chan, J. Greeley, V. Stamenkovic and N. M. Markovic, *Nat. Mater.*, 2012, **11**, 550–557.
110 Z. Lu, H. Wang, D. Kong, K. Yan, P. C. Hsu, G. Zheng, H. Yao, Z. Liang, X. Sun and Y. Cui, *Nat. Commun.*, 2014, **5**, 1–7.
111 R. D. L. Smith, *Science*, 2013, **340**, 60–63.
112 X. Xu, W. Liu, Y. Kim and J. Cho, *Nano Today*, 2014, **9**, 604–630.
113 H. Wang, Q. Zhang, H. Yao, Z. Liang, H. W. Lee, P. C. Hsu, G. Zheng and Y. Cui, *Nano Lett.*, 2014, **14**, 7138–7144.
114 Y. Li, Z. Cao, Y. Wang, B. Li, J. Yang and Z. Sun, *J. Colloid Interface Sci.*, 2024, **655**, 508–517.
115 W. Qiu, J. Jiao, J. Xia, H. Zhong and L. Chen, *Chem. - Eur. J.*, 2015, **21**, 4359–4367.
116 G. Huang, T. Chen, Z. Wang, K. Chang and W. Chen, *J. Power Sources*, 2013, **235**, 122–128.
117 J. Gautam, D. T. Tran, T. I. Singh, N. H. Kim and J. H. Lee, *J. Power Sources*, 2019, **427**, 91–100.
118 M. Guo, J. Du, X. Liu, W. Liu, M. Zhao, J. Wang and X. Li, *Molecules*, 2024, **29**, 3642.
119 S. Tao, W. Huang, H. Xie, J. Zhang, Z. Wang, W. Chu, B. Qian, L. Song, S. D. Wang, L. Zhang and J. F. Zhu, *RSC Adv.*, 2017, **7**, 39427–39433.
120 M. Shen, C. Ruan, Y. Chen, C. Jiang, K. Ai and L. Lu, *ACS Appl. Mater. Interfaces*, 2015, **7**, 1207–1218.
121 M. Guo, J. Balamurugan, T. D. Thanh, N. H. Kim and J. H. Lee, *J. Mater. Chem. A*, 2016, **4**, 17560–17571.
122 H. Schulenburg, S. Stankov, V. Schünemann, J. Radnik, I. Dorbandt, S. Fiechter, P. Bogdanoff and H. Tributsch, *J. Phys. Chem. B*, 2003, **107**, 9034–9041.
123 Y. Zhong, X. Xia, F. Shi, J. Zhan, J. Tu and H. J. Fan, *Adv. Sci.*, 2016, **3**, 1500286.
124 Y. C. Kimmel, X. Xu, W. Yu, X. Yang and J. G. Chen, *ACS Catal.*, 2014, **4**, 1558–1562.
125 Y. Xiao, J.-Y. Hwang and Y.-K. Sun, *J. Mater. Chem. A*, 2016, **4**, 10379–10393.
126 W. Yang, S. Rehman, X. Chu, Y. Hou and S. Gao, *ChemNanoMat*, 2015, **1**, 376–398.
127 L. Zhang, H. Yang, D. K. J. A. Wanigarathna and B. Liu, *Small Methods*, 2018, **2**, 1700353.
128 J.-S. Li, Y. Wang, C.-H. Liu, S.-L. Li, Y.-G. Wang, L.-Z. Dong, Z.-H. Dai, Y.-F. Li and Y.-Q. Lan, *Nat. Commun.*, 2016, **7**, 11204.
129 J. Su, G. Xia, R. Li, Y. Yang, J. Chen, R. Shi, P. Jiang and Q. Chen, *J. Mater. Chem. A*, 2016, **4**, 9204–9212.
130 Y. Liu, G. Yu, G. D. Li, Y. Sun, T. Asefa, W. Chen and X. Zou, *Angew. Chem., Int. Ed.*, 2015, **54**, 10752–10757.
131 K. Liu, Z. Peng, H. Wang, Y. Ren, D. Liu, J. Li, Y. Tang and N. Zhang, *J. Electrochem. Soc.*, 2017, **164**, F475–F483.
132 H. Jiang, Y. Yao, Y. Zhu, Y. Liu, Y. Su, X. Yang and C. Li, *ACS Appl. Mater. Interfaces*, 2015, **7**, 21511–21520.
133 X. Yang, X. Feng, H. Tan, H. Zang, X. Wang, Y. Wang, E. Wang and Y. Li, *J. Mater. Chem. A*, 2016, **4**, 3947–3954.
134 L. Zhang, H. Yang, D. K. J. A. Wanigarathna and B. Liu, *Small Methods*, 2018, 1700353.
135 J. H. Kim, J. Kim, J. H. Park, C. K. Kim, C. S. Yoon and Y. Shon, *Nanotechnology*, 2007, **18**, 115609.
136 P. Guo, G. Zhu, H. Song, X. Chen and S. Zhang, *Phys. Chem. Chem. Phys.*, 2011, **13**, 17818–17824.
137 Y. Leng, J. Li, C. Zhang, P. Jiang, Y. Li, Y. Jiang and S. Du, *J. Mater. Chem. A*, 2017, **5**, 17580–17588.
138 W. R. L. Lambrecht, M. S. Miao and P. Lukashev, *J. Appl. Phys.*, 2005, **97**, 1–4.
139 R. S. Ningthoujam and N. S. Gajbhiye, *Prog. Mater. Sci.*, 2015, **70**, 50–154.
140 Y. Zhong, X. Xia, F. Shi, J. Zhan, J. Tu and H. J. Fan, *Adv. Sci.*, 2016, **3**, 1500286.
141 B. Anasori, Y. Xie, M. Beidaghi, J. Lu, B. C. Hosler, L. Hultman, P. R. C. Kent, Y. Gogotsi and M. W. Barsoum, *ACS Nano*, 2015, **9**, 9507–9516.
142 J. Balamurugan, T. D. Thanh, N. H. Kim and J. H. Lee, *Adv. Mater. Interfaces*, 2016, **3**, 1500348.
143 H. Yin, C. Zhang, F. Liu and Y. Hou, *Adv. Funct. Mater.*, 2014, **24**, 2930–2937.
144 X. Li, Z. Ao, J. Liu, H. Sun, A. I. Rykov and J. Wang, *ACS Nano*, 2016, **10**, 11532–11540.
145 B. Gao, X. Li, X. Guo, X. Zhang, X. Peng, L. Wang, J. Fu, P. K. Chu and K. Huo, *Adv. Mater. Interfaces*, 2015, **2**, 1–9.
146 Y. Chen, T. Rao, J. Zhan, L. H. Zhang and F. Yu, *Chem. Commun.*, 2025, **61**, 7684–7687.
147 X. Shu, S. Chen, S. Chen, W. Pan and J. Zhang, *Carbon*, 2020, **157**, 234–243.
148 J. Tian, Q. Liu, Y. Liang, Z. Xing, A. M. Asiri and X. Sun, *ACS Appl. Mater. Interfaces*, 2014, **6**, 20579–20584.
149 Y. Liang, Q. Liu, A. M. Asiri, X. Sun and Y. Luo, *ACS Catal.*, 2014, **4**, 4065–4069.
150 Z. Jin, P. Li and D. Xiao, *Green Chem.*, 2016, **18**, 1459–1464.
151 S. T. Oyama, T. Gott, H. Zhao and Y. K. Lee, *Catal. Today*, 2009, **143**, 94–107.
152 Z. Pu, I. S. Amiinu, C. Zhang, M. Wang, Z. Kou and S. Mu, *Nanoscale*, 2017, **9**, 3555–3560.

153 M. Wang, C. Zhang, T. Meng, Z. Pu, H. Jin, D. He, J. Zhang and S. Mu, *J. Power Sources*, 2019, **413**, 367–375.
154 M. Zhuang, X. Ou, Y. Dou, L. Zhang, Q. Zhang, R. Wu, Y. Ding, M. Shao and Z. Luo, *Nano Lett.*, 2016, **16**, 4691–4698.
155 Y. Yang, X. Liang, F. Li, S. Li, X. Li, S.-P. Ng, C.-M. L. Wu and R. Li, *ChemSusChem*, 2018, 1–14.
156 D. Zhou and L.-Z. Fan, *J. Mater. Chem. A*, 2017, **6**, 2139–2147.
157 J. Hu, L. Peng, A. Primo, J. Albero and H. García, *Cell Rep. Phys. Sci.*, 2022, **3**, 100873.
158 L.-N. Zhang, S.-H. Li, H.-Q. Tan, S. U. Khan, Y.-Y. Ma, H.-Y. Zang, Y.-H. Wang and Y.-G. Li, *ACS Appl. Mater. Interfaces*, 2017, **9**, 16270–16279.
159 Z. F. Liu, *Wuli Huaxue Xuebao*, 2017, **33**, 1503–1504.
160 B. Liu, H. Li, B. Cao, J. Jiang, R. Gao and J. Zhang, *Adv. Funct. Mater.*, 2018, **28**, 1801527.
161 N. Heterocycles, X. Cui, Y. Li, S. Bachmann, M. Scalone and A. Surkus, *J. Am. Chem. Soc.*, 2015, **137**, 10652–10658.
162 Z. Xu, W. Li, Y. Zhang, Z. Xue, X. Guo and G. Zhang, *Ind. Eng. Chem. Res.*, 2016, **55**, 10591–10599.
163 Z. Song, W. Liu, W. Wei, C. Quan, N. Sun, Q. Zhou, G. Liu and X. Wen, *J. Alloys Compd.*, 2016, **685**, 355–363.
164 Y. Wang, S. Gai, N. Niu, F. He and P. Yang, *J. Mater. Chem. A*, 2013, **1**, 9083.
165 N. Zhou, Q. An, Z. Xiao, S. Zhai and Z. Shi, *RSC Adv.*, 2017, **7**, 45156–45169.
166 R. Ma, Z. Lu, C. Wang, H. E. Wang, S. Yang, L. Xi and J. C. Y. Chung, *Nanoscale*, 2013, **5**, 6338–6343.
167 M. Guo, J. Balamurugan, T. D. Thanh, N. H. Kim and J. H. Lee, *J. Mater. Chem. A*, 2016, **4**, 17560–17571.
168 W. Zhong, H. Liu, C. Bai, S. Liao and Y. Li, *ACS Catal.*, 2015, **5**, 1850–1856.
169 G. Wu, L. Zhao, M. Zong, P. Yu, J. Xie, Z. Da, H. Liu and J. Rong, *J. Colloid Interface Sci.*, 2022, **608**, 1278–1285.
170 R. Wang, X. Y. Dong, J. Du, J. Y. Zhao and S. Q. Zang, *Adv. Mater.*, 2018, **30**, 1703711.
171 M. Zeng, Y. Liu, F. Zhao, K. Nie, N. Han, X. Wang, W. Huang, X. Song, J. Zhong and Y. Li, *Adv. Funct. Mater.*, 2016, **26**, 4397–4404.
172 J. Balamurugan, T. D. Thanh, N. H. Kim and J. H. Lee, *Biosens. Bioelectron.*, 2016, **83**, 68–76.
173 X. Cui, Y. Li, S. Bachmann, M. Scalone, A. E. Surkus, K. Junge, C. Topf and M. Beller, *J. Am. Chem. Soc.*, 2015, **137**, 10652–10658.
174 Z. Wei, Y. Hou, X. Zhu, L. Guo, Y. Liu and A. Zhang, *ChemCatChem*, 2018, 310014.
175 K.-Y. Zhou, G.-Y. Chen, J.-A. Liu, Z.-P. Zhang, P. Sun, W.-Z. Zhang, F. Niu, W.-X. Zhang and J.-C. Liang, *RSC Adv.*, 2016, **6**, 90069–90075.
176 Z. Wei, Y. Chen, J. Wang, D. Su, M. Tang, S. Mao and Y. Wang, *ACS Catal.*, 2016, **6**, 5816–5822.
177 S. Lin, X. Shi, H. Yang, D. Fan, Y. Wang and K. Bi, *J. Alloys Compd.*, 2017, **720**, 147–155.
178 Y. Liu, J. Yuan, J. Zhou, K. Pan, R. Zhang, R. Zhao, L. Li, Y. Huang and Z. Liu, *Light Sci. Appl.*, 2024, **13**, 270.
179 Q. Zhang, H. Chen, X. Han, J. Cai, Y. Yang, M. Liu and K. Zhang, *ChemSusChem*, 2016, **9**, 186–196.
180 R. Cong, M. Jo, A. Martino, H. H. Park, H. Lee and C. S. Lee, *Sci. Rep.*, 2022, **12**, 16002.
181 M. Aadil, W. Shaheen, M. F. Warsi, M. Shahid, M. A. Khan, Z. Ali, S. Haider and I. Shakir, *J. Alloys Compd.*, 2016, **689**, 648–654.
182 X. Fan, Z. Peng, R. Ye, H. Zhou and X. Guo, *ACS Nano*, 2015, **9**, 7407–7418.
183 Y. Zhang, P. Wang, J. Yang, K. Li, X. Long, M. Li, K. Zhang and J. Qiu, *Chem. Eng. J.*, 2020, **401**, 126001.
184 J. Jin, X. Fu, Q. Liu and J. Zhang, *J. Mater. Chem. A*, 2013, **1**, 10538.
185 Z.-S. Wu, S. Yang, Y. Sun, K. Parvez, X. Feng and K. Müllen, *J. Am. Chem. Soc.*, 2012, **134**, 9082–9085.
186 J. Wang, G. Wang, S. Miao, J. Li and X. Bao, *Faraday Discuss.*, 2014, **176**, 135–151.
187 I. S. Amiinu, Z. Pu, X. Liu, K. A. Owusu, H. G. R. Monestel, F. O. Boakye, H. Zhang and S. Mu, *Adv. Funct. Mater.*, 2017, **27**, 1–11.
188 T. Liu, F. Yang, G. Cheng and W. Luo, *Small*, 2018, **14**, 1703748.
189 Z. Zhen, Z. Jiang, X. Tian, L. Zhou, B. Deng, B. Chen and Z.-J. Jiang, *RSC Adv.*, 2018, **8**, 14462–14472.
190 B. Chen, R. Li, G. Ma, X. Gou, Y. Zhu and Y. Xia, *Nanoscale*, 2015, **7**, 20674–20684.
191 H. J. Niu, L. Zhang, J. J. Feng, Q. L. Zhang, H. Huang and A. J. Wang, *J. Colloid Interface Sci.*, 2019, **552**, 744–751.
192 H. Liu, D. H. Yang, X. Y. Wang, J. Zhang and B. H. Han, *J. Colloid Interface Sci.*, 2021, **581**, 362–373.
193 Y. Wang, Y. Nie, W. Ding, S. G. Chen, K. Xiong, X. Q. Qi, Y. Zhang, J. Wang and Z. D. Wei, *Chem. Commun.*, 2015, **51**, 8942–8945.
194 J. Sen Li, Y. Wang, C. H. Liu, S. L. Li, Y. G. Wang, L. Z. Dong, Z. H. Dai, Y. F. Li and Y. Q. Lan, *Nat. Commun.*, 2016, **7**, 11204.
195 Y. Xu, W. Tu, B. Zhang, S. Yin, Y. Huang, M. Kraft and R. Xu, *Adv. Mater.*, 2016, **29**, 1605957.
196 J.-S. Li, J.-Q. Sha, B. Du and B. Tang, *Chem. Commun.*, 2017, **53**, 12576–12579.
197 S. Wang, H. Wang, C. Huang, P. Ye, X. Luo, J. Ning, Y. Zhong and Y. Hu, *Appl. Catal., B*, 2021, **298**, 120512.
198 K. Tang, L. Chen, Y. Xiong, L. Zhang and M. Wu, *ACS Appl. Nano Mater.*, 2023, **6**, 11553–11560.
199 S. Sun, F. Yang, X. Zhang, J. Qian, K. Wei, J. An, Y. Sun, S. Wang, X. Li and Y. Li, *Chem. Eng. J.*, 2024, **487**, 150673.
200 J. Quílez-Bermejo, A. Daouli, S. G. Dalí, Y. Cui, A. Zitolo, J. Castro-Gutiérrez, M. Emo, M. T. Izquierdo, W. Mustain, M. Badawi, A. Celzard and V. Fierro, *Adv. Funct. Mater.*, 2024, **34**, 2403810.
201 B. N. V. Krishna, O. R. Ankinapalli, A. R. Reddy and J. S. Yu, *Small*, 2023, **20**, 2311176.
202 Y. Pan, Y. Li, A. Nairan, U. Khan, Y. Hu, B. Wu, L. Sun, L. Zeng and J. Gao, *Adv. Sci.*, 2023, **11**, 2308205.
203 S. Ramakrishnan, D. B. Velusamy, S. Sengodan, G. Nagaraju, D. H. Kim, A. R. Kim and D. J. Yoo, *Appl. Catal., B*, 2021, **300**, 120752.

204 D. Zhao, Y. Zhu, Q. Wu, W. Zhou, J. Dan, H. Zhu, W. Lei, L. J. Ma and L. Li, *Chem. Eng. J.*, 2021, **430**, 132825.
205 G. Zhou, G. Liu, X. Liu, Q. Yu, H. Mao, Z. Xiao and L. Wang, *Adv. Funct. Mater.*, 2022, **32**, 2107608.
206 L. Xu, Z. Mao, J. Liu, M. Bi, T. Tu, Y. Tian, X. Zhou, J. Wu, Y. Wu, J. Su, S. Chen and H. Yin, *Adv. Energy Mater.*, 2025, **15**, 2501790.
207 Y. Yao, C. Zhang, W. Wei, H. Wang, Z. Liu, Y. Jin and J. Ma, *J. Energy Storage*, 2025, **132**, 117850.
208 T. Huang, J. Xiao, X. Liu, Y. Feng, J. He, G. Xu and L. Zhang, *Small*, 2025, **21**, 2506911.
209 D. I. Jeong, U. Y. Lee, H. Kim, H. S. Bang, H. W. Choi, J. Kim, H. G. Choi, H. S. Oh, B. K. Kang and D. H. Yoon, *Small*, 2024, **20**, 2307830.
210 J. Su, N. Jiang, Y. Wang, B. Jiang, X. Wang and H. Song, *Energy*, 2025, **318**, 134905.
211 M. Muthamildevi, D. Thiruvengadam, K. Umapathy, M. Sangamithirai, K. Rajan, M. Vijayarangan and J. Jayabharathi, *Energy and Fuels*, 2024, **38**, 11161–11171.
212 Y. Wang, Y. Zhang, P. Xing, X. Li, Q. Du, X. Fan, Z. Cai, R. Yin, Y. Yao and W. Gan, *Adv. Mater.*, 2024, **36**, 2402391.
213 X. Wang, Z. Qin, J. Qian, L. Chen and K. Shen, *Appl. Catal., B*, 2024, **359**, 124506.
214 P. Bai, P. Wang, J. Mu, Y. Zhao, C. Du and Y. Su, *Appl. Catal., B*, 2024, **349**, 123882.
215 T. D. Le, D. S. Kim, G. J. Oh, G. S. Shin, T. Van Tran, B. G. Ahn and Y. T. Yu, *Sustain. Mater. Technol.*, 2024, **41**, e01068.
216 S. Min, Y. Zhao, Z. Meng, F. Wang, W. Li and Z. Zhang, *Renewable Energy*, 2024, **41**, 121383.
217 R. J. Bani, J. Mishra, S. Pratihar, R. Patidar, D. N. Srivastava and G. R. Bhadu, *Sustain. Energy Fuels*, 2026, **10**, 1480–1494.
218 Y. Cao, Y. Yan, Y. Wen, M. Cao, Y. Li, H. Xie and W. Gu, *Inorg. Chem.*, 2024, **63**, 3599–3609.
219 J. Liu, Z. Luo, J. Wu, D. Qian, W. Liao, G. I. N. Waterhouse and X. Chen, *Inorg. Chem.*, 2024, **63**, 12681–12689.
220 Z. Pei, T. Qin, W. Wang, T. Li and X. Guo, *ACS Appl. Mater. Interfaces*, 2025, **17**, 62205–62216.
221 X. W. Lv, W. S. Xu, W. W. Tian, H. Y. Wang and Z. Y. Yuan, *Small*, 2021, **17**, 2101856.
222 R. Jena, S. Bhattacharyya, N. Bothra, V. Kashyap, S. K. Pati and T. K. Maji, *ACS Appl. Mater. Interfaces*, 2023, **15**, 27893–27904.
223 J. Liu, J. Zhou and M. K. H. Leung, *ACS Appl. Mater. Interfaces*, 2022, **14**, 4399–4408.
224 L. Zhang, Y. Zhu, Z. Nie, Z. Li, Y. Ye, L. Li, J. Hong, Z. Bi, Y. Zhou and G. Hu, *ACS Nano*, 2021, **15**, 13399–13414.
225 D. H. Park, Y. S. Kim, S. B. Han, W. J. Lee, H. J. Lee, Y. S. Lee, S. H. Moon and K. W. Park, *Int. J. Hydrogen Energy*, 2021, **46**, 22499–22507.
226 S. Seok, M. Choi, Y. Lee, D. Jang, Y. Shin, Y. H. Kim, C. Jo and S. Park, *ACS Appl. Nano Mater.*, 2021, **4**, 9418–9429.
227 W. Yang, J. Guo, J. Ma, N. Wu, J. Xiao and M. Wu, *J. Alloys Compd.*, 2022, **926**, 166937.
228 R. Guo, J. Shi, L. Hong, K. Ma, W. Zhu, H. Yang, J. Wang, H. Wang and M. Sheng, *ACS Appl. Mater. Interfaces*, 2022, **14**, 56847–56855.
229 Q. P. Ngo, T. T. Nguyen, M. Singh, N. H. Kim and J. H. Lee, *J. Mater. Chem. A*, 2023, **12**, 1185–1199.
230 P. Arunkumar, S. Gayathri and J. H. Han, *ChemSusChem*, 2021, **14**, 1921–1935.
231 L. Yi, B. Feng, N. Chen, W. Li, J. Li, C. Fang, Y. Yao and W. Hu, *Chem. Eng. J.*, 2021, **415**, 129034.
232 L. Xu, S. Wu, X. He, H. Wang, D. Deng, J. Wu and H. Li, *Chem. Eng. J.*, 2022, **437**, 135291.
233 Z. Cao, P. Li, H. Guan, W. Yang, Y. Liu, C. Tian, W. Zhao, Q. Dong, C. A. Wang and Z. Xie, *Int. J. Hydrogen Energy*, 2024, **95**, 156–164.
234 W. Duan, C. Wang, P. Sun, Y. Sun, Y. Zhuang, J. Wang and Z. Li, *ACS Appl. Nano Mater.*, 2023, **6**, 16662–16673.
235 X. Zhang, X. Wen, C. Pan, X. Xiang, C. Hao, Q. Meng, Z. Q. Tian, P. K. Shen and S. P. Jiang, *Chem. Eng. J.*, 2021, **431**, 133216.
236 H. L. Meng, S. Y. Lin, J. J. Feng, L. Zhang and A. J. Wang, *J. Colloid Interface Sci.*, 2022, **610**, 573–582.
237 C. Zhang, J. Liu, Y. Ye, Q. Chen and C. Liang, *Carbon*, 2020, **156**, 31–37.
238 W. Wan, S. Wei, J. Li, C. A. Triana, Y. Zhou and G. R. Patzke, *J. Mater. Chem. A*, 2019, **7**, 15145–15155.
239 S. Ramakrishnan, J. Balamurugan, M. Vinothkannan, A. R. Kim, S. Sengodan and D. J. Yoo, *Appl. Catal., B*, 2020, **279**, 119381.
240 U. P. Suryawanshi, U. V. Ghorpade, D. M. Lee, M. He, S. W. Shin, P. V. Kumar, J. S. Jang, H. R. Jung, M. P. Suryawanshi and J. H. Kim, *Chem. Mater.*, 2021, **33**, 234–245.
241 X. Han, N. Li, P. Xiong, Y. Kang, Q. Dou, Q. Liu, W. Li, J. Y. Lee and H. S. Park, *Composites, Part B*, 2022, **234**, 109670.
242 Y. Feng, X. Y. Yu and U. Paik, *Sci. Rep.*, 2016, **6**, 34004.
243 X. Cui, P. Ren, D. Deng, J. Deng and X. Bao, *Energy Environ. Sci.*, 2016, **9**, 123–129.
244 M. Nozari-Asbemarz, H. Imanzadeh, L. Hazraty, B. Babaei, A. Abbasi, S. S. Mehrabi-Kalajahi, M. A. Vafolomeev, J. J. Leahy and M. Amiri, *J. Power Sources*, 2025, **652**, 237555.
245 L. Zhang, C. Chang, C.-W. Hsu, C.-W. Chang and S.-Y. Lu, *J. Mater. Chem. A*, 2017, **5**, 19656–19663.
246 X. Cui, P. Ren, D. Deng, J. Deng and X. Bao, *Energy Environ. Sci.*, 2016, **9**, 123–129.